Tracking RPE Transplants Labeled by Retroviral Gene Transfer with Green Fluorescent Protein

Chi-Chun Lai,[1] Peter Gouras,[1] Ken Doi,[1] Fang Lu,[1] Hild Kjeldbye,[1] Steven P. Goff,[2] Robert Pawliuk,[4] Philippe Leboulch,[3] and Stephen H. Tsang[2,5]

Purpose. To determine whether human retinal pigment epithelium (RPE) can be modified by retroviral-mediated gene transfer and to monitor the human RPE cells in the subretinal space of living rabbits with scanning laser ophthalmoscopy (SLO).

Methods. Cultured human fetal retinal pigment epithelium (HFRPE) was exposed to green fluorescent protein (GFP)-transducing retroviral vectors, Moloney murine leukemia virus, and lentivirus. The cultured cells were followed by fluorescence microscopy. Suspensions of GFP-expressing HFRPE were transplanted into the subretinal space of pigmented rabbits, and the transplant sites were examined by SLO for fluorescence, including fluorescein and indocyanine green angiography. The rabbits were euthanatized at different times after transplantation, and the retinas were studied histologically.

Results. Retroviral gene transfer can introduce a foreign gene such as GFP into cultured HFRPE. Gene expression is maintained in cultured RPE for at least 3 months. The lentiviral vector traduced both nondividing and dividing cells; the Moloney vector only transduced the latter. GFP-expressing cells can be followed in the living retina. Their changes reflect the rejection response followed histologically.

Conclusions. Cultured HFRPE could be transduced to express GFP for long periods of time by retroviral gene transfer. GFP allowed retinal transplants and gene expression to be monitored in vivo. These results provide a model for potential ex vivo gene therapy in the subretinal space. (*Invest Ophthalmol Vis Sci.* 1999;40:2141–2146)

From the [1]Departments of Ophthalmology and [2]Biochemistry, and Molecular Biophysics, Columbia University, Howard Hughes Medical Institute, New York, New York; [3]Harvard Medical School; Massachusetts Institute of Technology; [4]Genetix Pharmaceuticals, Inc., Cambridge, Massachusetts; and [5]The Jules Stein Eye Institute, UCLA, Los Angeles, California.

Supported by The Foundation Fighting Blindness, a National Institutes of Health Grants EY RO1-EY03854 (PG) and %32 EY07105 (SHT), and by a fellowship (KD) from the International Human Frontier Science Program, and Fight for Sight, Research Division of Prevent Blindness (SHT). S. P. Goff is an investigator of the Howard Hughes Medical Institute.

Submitted for publication October 8, 1998; revised March 8, 1999; accepted April 8, 1999.

Proprietary interest category: P.

Reprint requests: Peter Gouras, Columbia University, Department of Ophthalmology, 630 West 168th Street, New York, NY 10032.

The green fluorescent protein (GFP) gene has been derived from the bioluminescent jelly fish, *Aequorin victoria*. This protein fluoresces green light when excited by blue or ultraviolet light. The cloning of this gene and the demonstration that it can be expressed in other organisms provides a useful way to select and follow cells exhibiting specific gene expression,[1–3] especially in a transparent structure such as the eye.[4]

We have used replication-deficient retroviruses to transduce cultured human fetal retinal pigment epithelium (HFRPE) with the gene encoding GFP. We followed the expression of this protein in vitro by fluorescence microscopy and in vivo after transplantation to the subretinal space of rabbits by scanning laser ophthalmoscopy (SLO). We demonstrated that retroviral transduction is effective, stable, and long-lasting in vitro. It allows transplanted RPE to be monitored in the subretinal space and provides a noninvasive indicator of the time course of rejection. An abstract on some of this research has been published.[5]

Methods

Culturing of RPE

Donor tissue was obtained from human fetal eyes, 16 to 20 weeks of gestational age. Informed consent was obtained for the use of this tissue before abortion and institutional approval was granted through an agreement between Albert Einstein College of Medicine, the source of the tissue, and Columbia University. The eye bulbs were washed externally with 70% alcohol and then with phosphate-buffered saline (PBS). The eyes were put into our standard RPE culture medium, Dulbecco's modified Eagle's medium with 4.5 g/l glucose supplemented with 20% fetal calf serum (Hyclone, Logan, Utah), 2 mM L-glutamine and penicillin (50 unit/ml)/streptomycin (50 mg/ml) (Gibco, Grand Island, NY). The anterior segment with lens, vitreous, and neural retina was removed. The posterior segment was sliced into quadrants, and RPE patches were separated gently from Bruch's membrane and choroid, using fine forceps and microscopic viewing. A distinct cleavage plane is identifiable between the taut monolayer patch of RPE and the adjacent choroid so that an isolated sheet of RPE can be pulled off. Each sheet was placed in a separate culture plate. The edges of the sheet were pressed onto the surface of the plate with the tip of a 26-gauge needle. The cultures were maintained at 37°C in an incubator with a humidified atmosphere of 95% air/5% CO_2, fed every 3 to 4 days, and examined almost daily. To obtain cell suspensions, we washed the cells with PBS three times and exposed them to 2.5% trypsin in Hank's solution with EDTA without Ca and Mg (Gibco) for 10 minutes at 37°C. The monolayer was triturated into single cells or clusters of cells by repeated pipetting. The concentration of cells in a suspension was determined with a hemocytometer. The cells were either used for transplantation or subcultured.

Preparation of Virus Stocks

For the Moloney vector a DNA construct was generated consisting of the humanized red-shifted GFP (EGFP) under the translational control of an Internal Ribosome Entry Site from the encephalomyocarditis virus (EMCV-IRES), flanked by long terminal repeat (LTR) of Moloney murine leukemia virus (MoMLV). These viral sequences include the two LTRs, and the two sites for initiation of viral DNA synthesis (the primer binding site for initiation of minus-strand DNA synthesis and the polypurine tract for initiation of plus-strand synthesis). They also include the RNA packaging signal, termed the Psi region, near the 5′ end of the genome.

The construct was then introduced into AM 12 packaging cells that express the viral proteins required for the assembly of a virion particle. The viral RNA was transcribed from a transfected plasmid and selectively packaged into viral particles produced by the packaging cells. The virions were collected from the culture medium, purified, and concentrated as needed. To transduce the gene to RPE, the virus was applied directly to the target cells. Typical titers were 10^5 to 10^6 infectious units/ml.

For the lentiviral vector, human immunodeficiency virus (HIV)-based preparations were generated by cotransfection of human kidney–derived 293T cells by three plasmids using the $CaPO_4$ method.[6] The packaging construct contained the cytomegalovirus promoter and the insulin polyadenylation signal to express all the viral proteins in *trans,* except the envelope and Vpu.[6] The second plasmid provided a vector with all the *cis*-acting elements that allow transfer and integration into the target cell. In this transducing vector, an expression cassette with the Rev responsive element (RRE) and the cytomegalovirus promoter are used to direct the expression of GFP.[6] The third plasmid provides the envelope protein from the vesicular stomatitis virus glycoprotein to enhance the viral stability and the range of possible target cells.[6] The titer of the HIV vector was determined by a fluorescent activated cell sorter (FACStar plus; Becton Dickinson, Mountain View, CA) scanning GFP-transduced cells. The lentiviral titers were determined by infection of 293 cells seeded in 6-well plates at 1×10^5 cells per well the day before infection with serial dilution of concentrated viral stock in the presence of 8 μg/ml of polybrene (Aldrich, Milwaukee, WI). After overnight incubation, the cell culture medium was changed, and the cells were incubated further for 2 days. GFP fluorescent cells were identified by fluorescent microscopy and/or the FACS. Typical titers were 10^8 to 10^9 infectious units/ml.

In Vitro Transfection

For viral transduction, primary cultures were dissociated into cell suspensions and subcultured in 6-well plates containing approximately 10^5 cells/well. This promotes cell division and augments the total number of cells available. After 24 hours in standard RPE culture medium, the medium was replaced with the viral solution, consisting of Hepes buffer with 20% fetal calf serum, 2 mM L-glutamine, 8 μg/ml polybrene, and a viral titer of 10^5 to 10^7 infectious units/ml before concentration. This solution was replaced with fresh viral solution every 6 hours for 48 hours. After 48 hours, this solution was replaced with standard RPE medium, and the cultures were allowed to reach confluency, examined by fluorescence microscopy, and used for transplantation.

For comparing viral transduction of stationary versus dividing cells, the virus was introduced directly into the primary culture containing the original patch of heavily pigmented cells, surrounded by an expanding population of dividing cells, the size of which depended on the age of the culture. To determine the fraction of cells expressing GFP, the number of GFP fluorescent cells and the total number of cells were counted within defined areas, 0.4×0.8 mm, in the culture plate. All cells that showed green fluorescence were considered to be expressing GFP. We examined cells in the same areas in three different parts of each culture plate, the patch that contained stationary pigmented cells only, the edge of the patch where cells were migrating and entering into cell division, and the growing margin of the culture, which contained many fewer pigmented, dividing cells. We measured these same areas repeatedly in 15 different cultures, weekly for 3 weeks; 5 cultures were measured for 6 weeks, and 1 culture for 3 months. In one case, we dissociated a primary culture that we had examined for 3 months and replated the cells to follow GFP fluorescence after repeated cell division.

Transplantation

Thirty adult pigmented rabbits received subretinal transplants placed within small bleb detachments just below the myelinated region of the optic nerve. Bleb detachments also were formed in two rabbits with saline alone. Each animal was anesthetized with sodium pentobarbital (25 mg/kg, intramuscularly) and xylazine (10 mg/kg, intramuscularly). The pupil was dilated with 2% cyclopentolate and 2.5% neosynephrine. A lid speculum was used to keep the eye open and occasionally a canthotomy also was performed. A conjunctival flap was formed at the limbal region, and a sclerotomy made approximately 3 mm behind the limbus. A glass pipette with a tip diameter of 80 to 100 μm, connected to a 1-ml syringe and filled with balanced salt solution (BSS) was introduced into the vitreal cavity. Using a corneal contact lens and a surgical microscope the pipette was directed to the retinal surface. At the surface of the retina a jet stream of BSS was slowly injected through the neural retina to produce a small bleb detachment. A second similar pipette was used to suck up a pellet of a concentrated solution of GFP-expressing HFRPE cells from the bottom of an Eppendorf tube. The cell suspension was obtained by rinsing a culture three times with PBS and then dissociating the cells with 0.05% trypsin for 5 minutes at 37°C. The cells were washed with PBS and centrifuged. The pellet was resuspended in 0.5 ml BSS, put into an Eppendorf tube, centrifuged at 1000 rpm for 2 minutes, and stored at 4°C. The cells were used within 2 hours of preparation. Approximately 10 μl of cell suspension containing approximately 10^5 cells was introduced into the bleb detachment, either through the same retinotomy or through a second one; the latter method was preferable because it minimized any reflux of transplant cells into the vitreous. A small air bubble separated the suspension from the BSS solution in the pipette. The bubble also was introduced into the bleb detachment to prevent efflux of the transplant cells into the vitreous. The air bubble disappeared in 24 hours. After the pipette was removed, the sclera and conjunctiva were sutured with 9-0 nylon.

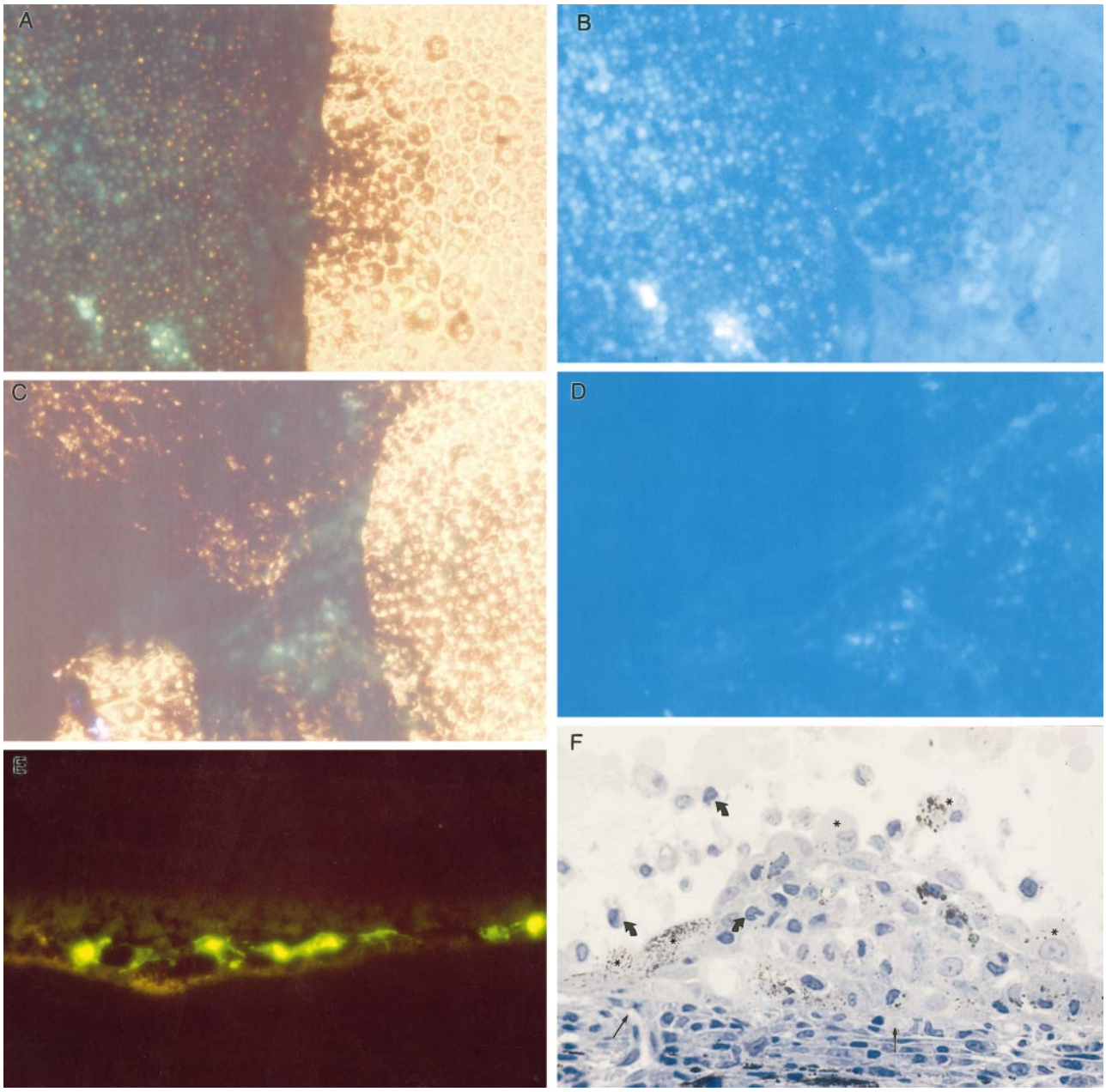

FIGURE 1. Color photographs of cultured HFRPE transfected with the GFP gene by Lentivirus 6 weeks previously. (**A**) An HFRPE patch culture (on the *left*) spreading out across the culture plate (on the *right*) photographed by both fluorescent and transmitted white light. Strong green fluorescence is visible on the left. (**B**) The same area as (**A**), photographed by fluorescence only. Both stationary (*left*) and dividing (*right*) cells show GFP fluorescence. (**C**) A HFRPE patch culture that shows no fluorescence (*upper left*) except along its border with cells migrating from its edge. (**D**) The same area as (**C**), photographed by fluorescence only. There is no fluorescence in the *upper left*, which appears identical with control cultures never exposed to the virus. GFP fluorescence is seen only along the edge of this patch and in the dividing cells (*right*). (**E**) GFP fluorescent HFRPE transplanted to the subretinal space of rabbit 1 week earlier. (**F**) Histologic section, stained with toluidine blue, showing cellular inflammation in a transplant site at 9 days after surgery. *Asterisks*, RPE cells with melanin; *curved arrows*, monocytes; *straight arrows*, rare choriocapillary.

Retinal Examination

Rabbits were examined 1 day after surgery, weekly for 8 weeks, and monthly thereafter by indirect ophthalmoscopy, SLO (Rodenstock, Munich, Germany) and sometimes by contact lens biomicroscopy. The SLO provided infrared (780 nmoles), He-Neon red (633 nmoles), argon green (514 nmoles), and blue (488 nmoles) illumination. We examined retinal fluorescence with argon blue illumination and a fluorescein barrier filter. We graded the fluorescence using a scale of 0 to 4 (0, no fluorescence,; 1, just detectable; 2, distinct; 3, strong; 4, very strong). Fluorescein and indocyanine green (ICG) angiography were performed simultaneously with an SLO double-detection system that was able to detect fluorescein and ICG simultaneously. Angiography was performed

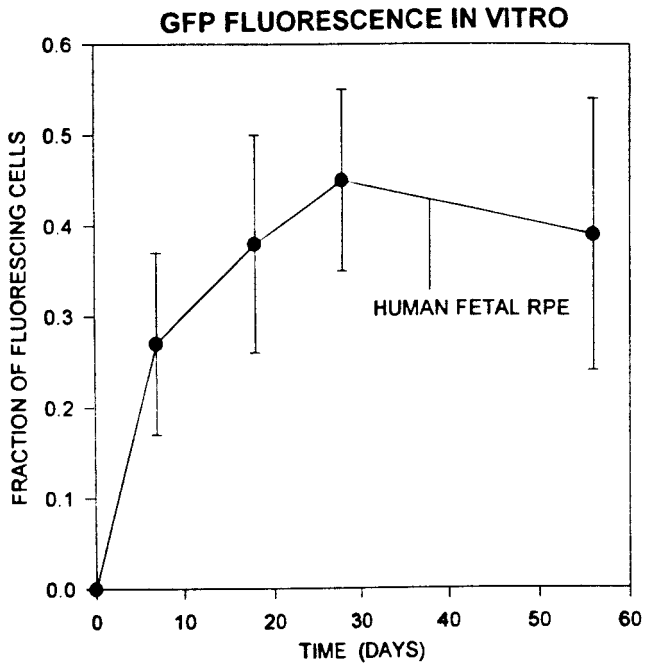

FIGURE 2. The relationship between the fraction of cultured HFRPE-expressing GFP fluorescence at different times after transduction with Lentivirus. Each *data point* is the average of measurements made in three different areas of 10 separate cultures; the vertical lines show the standard errors of the mean.

weekly for 2 to 3 weeks and monthly thereafter. The dyes were injected into an ear vein in one bolus containing 0.2 ml fluorescein (100 mg/ml) and 0.7 ml ICG (4.2 mg/ml).

Histology

After the rabbit was euthanatized, the eyes were enucleated, punctured with a 20 gauge needle at several places near the limbus to facilitate diffusion, and immersed in a solution of either 3% glutaraldehyde or 4% paraformaldehyde in PBS at pH 7.2 for 24 to 48 hours at 4°C. The eyes then were washed with PBS and dissected with the aid of a microscope. The transplant site was located, examined, and cut out with its orientation marked so that the site could be reached with minimal sectioning. For Epon embedding, glutaraldehyde-fixed segments were postfixed with 1% osmic acid and dehydrated with ethanol. Sections were cut semi-serially and examined by light microscopy; selected areas were examined by electron microscopy. For cryosectioning paraformaldehyde-fixed segments were immersed in OCT compound (Miles, Elkhart, IN) and frozen by dry ice. Cryosectioning was performed on a Leica 1850 cryotome (Leica Instruments, Nusslach, Germany). Sections were mounted on gelatinized glass slides with fluoromount-G. GFP polyclonal antibody (diluted 1:100; Clontech Laboratories, Palo Alto, CA) was used for immunocytochemistry. Cultured RPE cells not exposed to the virus were used as a negative control.

RESULTS

GFP fluorescence was detectable in cultured HFRPE within 5 days after being exposed to the retrovirus. The MoMLV only transduced dividing cells that occurred along the edge of patch cultures spreading out centrifugally over the culture plate.[7] The lentivirus transduced both stationary and dividing cells. Figure 1 shows heavily pigmented stationary cells within a patch culture and more lightly pigmented dividing cells spreading our from this patch, viewed by both fluorescent and transmitted white light, 6 weeks after exposure to Lentivirus. Figure 1B shows only the fluorescence of the same area. Green fluorescence can be seen in both the stationary and dividing cells. Figure 1C shows a heavily pigmented patch of stationary cells, which do not show any fluorescence (upper left). These cells appear identical with controls that have not been exposed to

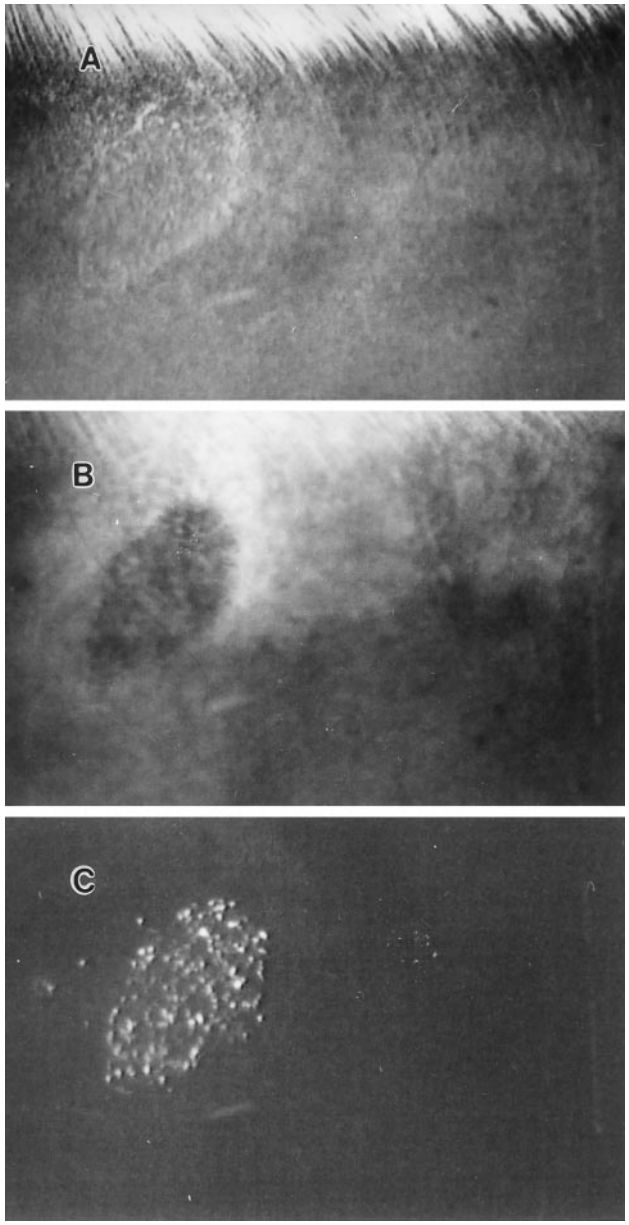

FIGURE 3. A transplant site in rabbit retina seen by SLO one week after surgery. The transplant site is the oval-like structure on the left with its upper edge just under the myelinated optic nerve fibers (seen best in **A**). (**A**) Red light image shows the transplant mainly by a light border that surrounds it. (**B**) Infrared image shows the transplant as a darker granular structure that stands out in the lighter normal retina. (**C**) Fluorescence image that reveals the GFP-positive cells in the transplant.

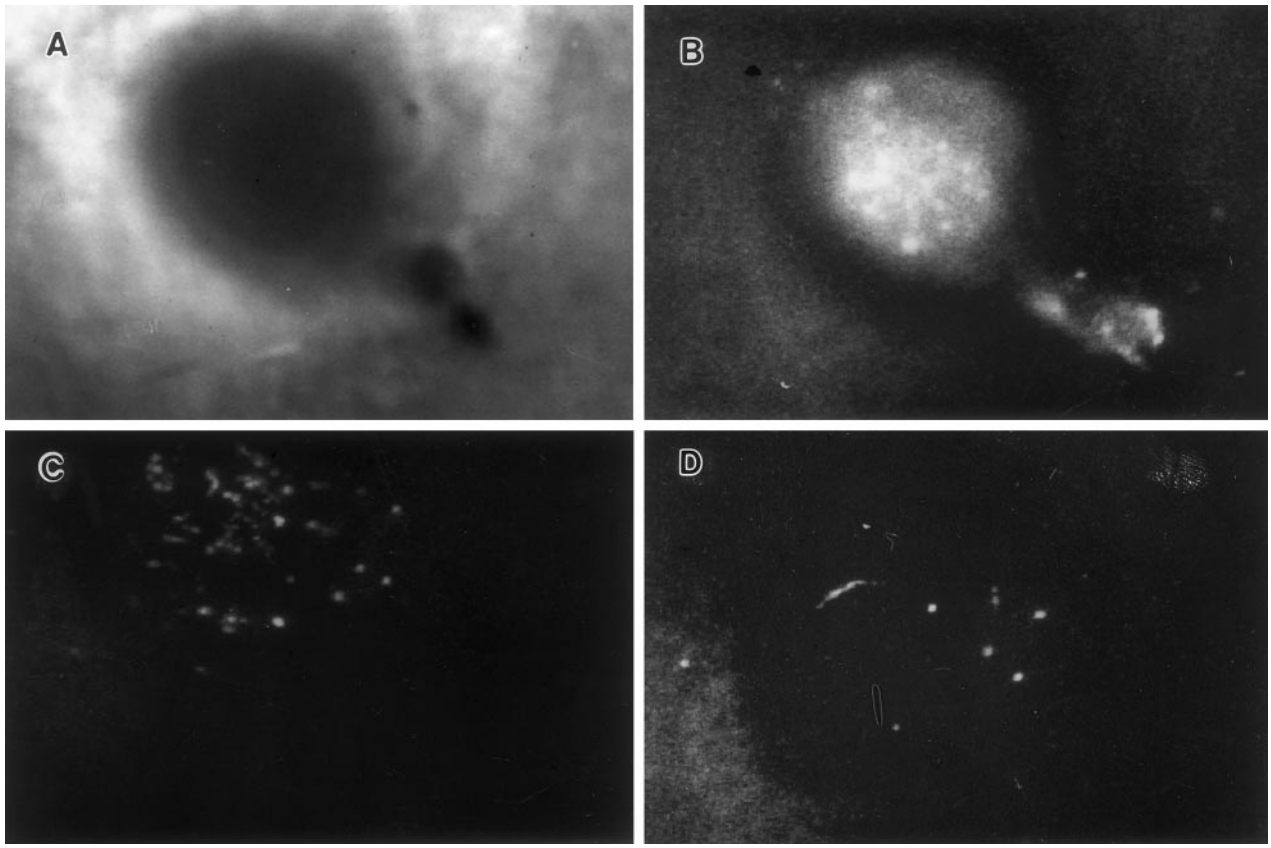

FIGURE 4. SLO photographs of an HFRPE xenograft in rabbit retina observed with infrared (**A**) and fluorescence (**B**) illumination at 5 days after surgery. The appearance of the transplant by fluorescence illumination at 9 days (**C**) and 2 weeks (**D**) after surgery shows a progressive diminution in the number of GFP fluorescent cells.

the virus. The fluorescence seen in this culture (Fig. 1D) occurs only at the edge of the patch and in the lightly pigmented cells migrating away from the patch. Subcultured cells continue to express GFP. The overall level of expression remained relatively stable for a 3-month period of observation. Immunohistochemistry confirmed the presence of GFP protein in the cultured RPE. Figure 2 shows the fraction of HFRPE cells expression detectable GFP fluorescence in vitro for 2 months. Approximately 30% of the cultured cells showed expression of high level of GFP fluorescence within the first week after exposure to the virus. This fraction slowly increased during the first month to reach approximately 45%.

Figure 3 shows an HFRPE transplant in the subretinal space of pigmented rabbit retina at 1 week after surgery by visible (red) (A) and infrared (B) illumination and fluorescence SLO (C). The transplant was better seen as a dark subretinal structure by infrared than by visible illumination; even its overall thickness can be estimated by its absorption of infrared light. Fluorescence revealed the GFP-expressing cells within the transplant. The dimensions of these bright structures with relatively sharp outlines approximated those of either single cells or small groups of cells. The fluorescent cells are congruent with the dark subretinal transplant seen by infrared illumination. The transplanted cells fill the area of the original bleb detachment visible by a dim demarcation line seen better by visible than infrared illumination.

Figure 4 shows a transplant site at 5 days after surgery by infrared (A) and fluorescence SLO (B, C, D). At 5 days, many GFP-fluorescing cells can be seen in the center of the transplant (Fig. 3B). At 9 days after surgery, many fluorescent cells have disappeared (Fig. 3C). At 2 weeks very few fluorescent cells remain. After 3 to 4 weeks, GFP fluorescence could not be detected in these transplants. There was a steady decrease in the amount of GFP fluorescence in these transplants with time after transplantation surgery.

Histology revealed GFP fluorescent cells in the subretinal space within 1 week after transplantation surgery (Fig. 1E). Between 1 and 3 weeks after surgery, the transplant site showed signs of rejection (Fig. 1F), and GFP-fluorescing cells became difficult to find. There was a dense concentration of monocytic cells in the choroid adjacent to the transplant site. The high concentration of inflammatory cells appeared to fill and/or compress the choroidal vessels and the choriocapillaries. Despite this intense inflammatory response in the choroid, there was no evidence of staining or leakage of dye during fluorescein and ICG angiography performed repeatedly in every rabbit.

DISCUSSION

Replication deficient retroviruses can introduce a foreign gene into HFRPE in vitro. This gene remains able to express a unique protein, in this case GFP, at a relatively constant rate for long periods of time, at least 3 months. Lentivirus was a more effective vector than MoMLV because it transduced both non-

dividing as well as dividing cells. MoMLV only transduced the latter. RPE patch cultures provide an easily identifiable and discrete group of cells that show no evidence of division. Cells within such patches retain the same appearance and pigmentation and do not increase in number for months. Dividing cells are easy to identify by their progressive loss of pigmentation, their continuous migration away from the edge of the patch, and their increase in numbers.[7] Therefore, human fetal RPE provides a good system to examine the transduction of dividing versus stationary, presumably nondividing, cells in vitro.

The variation in GFP fluorescence among the cells may be due to different sites of chromosomal integration, assuming this occurs. It also may be due to multiple integration and/or expression sites within the same cell. The fact that GFP expression is continuously maintained after subculturing and repeated cell division suggests that chromosomal integration has occurred. This can be better tested by Southern blot analysis or polymerase chain reaction of the GFP gene in genomic DNA.

GFP exhibits a strong, nonquenchable fluorescence that is easy to monitor by SLO viewing. Single transplanted cells or small groups of cells can be distinguished and followed noninvasively and long term. In our experiments, GFP-expressing HFRPE was transplanted into the subretinal space of rabbits, therefore, as xenografts. This led to rejection usually within 1 to 3 weeks after transplantation surgery. GFP-fluorescent cells were identifiable within the subretinal space in relatively large numbers within the first week after transplantation, but their numbers began to diminish as rejection progressed. The changes in GFP fluorescence followed the time course of the rejection process observed histologically. Therefore, GFP expression provided an in vivo monitor of the viability and gene expression of transplanted RPE.

The fact that a substantial number of cells do not show fluorescence reduces the sensitivity of the technique. This can be improved by FACS just before transplantation. On the other hand, GFP fluorescence appears to be specific for the transplanted cells because all trace of its fluorescence disappears after the transplant is rejected. Host rejection has prevented testing the long-term expression of these cells in vivo. This can be done by using allografts or homografts rather than xenografts in the future.

We found that GFP is an excellent monitor of not only the viability but also the function of the transplanted RPE, as manifest by gene expression and protein synthesis. By using this marker, one can track the presence of cells placed in the subretinal space and also monitor whether they are expressing a potentially therapeutic gene linked in tandem to the expression of GFP. The fact that RPE can be cultured easily provides a way to optimize the expression of a particular gene in vitro before it is introduced into the subretinal space. The question of rejection could of course be eliminated by using autografts such as cultured iris pigment epithelium from the same subject who is the target of such ex vivo form of gene therapy. Future engineering of RPE cells by retroviral vectors will undoubtedly augment their use in transplantation. In addition a marker that can be used to identify transplanted cells in the retina ophthalmoscopically will facilitate determining whether certain RPE allografts can survive in the subretinal space of human subjects without immunosuppression.[8]

Acknowledgments

The authors thank Inder M. Verma of the Salk Institute, La Jolla, California, for his generous contribution of the plasmids for establishing the Lentivirus vector, and Dorothy Warburton and Karen Weidenheim for their assistance.

References

1. Shimomura O, Johnson FH, Saiga Y. Extraction, purification and properties of aequorin, a bioluminescent protein from the luminous hydromedusan, Aequorea. *J. Cell Comp Physiol.* 1962;59: 223–227.
2. Prasher DC, Eckenrode VK, Ward WW, Prendergast FG, Cormier MJ. Primary structure of the Aequorea victoria green fluorescent protein. *Gene.* 1992;111:229–233.
3. Chalfie M, Tu Y, Euskirchen G, Ward WW, Prasher DC. Green fluorescent protein as a marker for gene expression. *Science.* 1994;263:802–805.
4. Bennett J, Duan D, Engelhardt JF, Maguire AM. Real-time, noninvasive in vivo assessment of Adeno-asoociated virus-mediated retinal transduction. *Invest Ophthalmol Vis Sci.* 1997;38:2857–2863.
5. Lai C, Pawliuk R, Gouras P, Tsang S, Lu F, Doi K, et al. Genetically engineered human RPE transplants express green fluorescent protein in the subretinal space[ARVO Abstract]. *Invest Ophthalmol Vis Sci.* 1998;39(4):**S**19. Abstract nr 73.
6. Naldini L, Blomer U, Gallay P, et al. In vivo gene delivery and stable transduction of nondividing cells by a Lentiviral vector. *Science.* 1996;272:263–267.
7. Gouras P, Cao H, Sheng, Y, Tanabe T, Efremova Y, Kjeldbye H. Patch culturing and transfer of human fetal retinal epithelium. *Graefes Arch Clin Exp Ophthalmol.* 1994;232:599–607.
8. Algvere P, Berglin L, Gouras P, Sheng Y, Dafgard Kopp E. Transplantation of RPE in age-related macular degeneration: observations in disciform lesions and dry RPE atrophy. *Graefes Arch Clin Exp Ophthalmol.* 1997;235:149–158.

Corneal Epithelial–Specific Cytokeratin 3 is an Autoantigen in Wegener's Granulomatosis–Associated Peripheral Ulcerative Keratitis

Irena Reynolds,[1] *Andrew B. Tullo,*[2] *Sally L. John,*[3] *P. J. Lennox Holt,*[1] *and M. Chantal Hillarby*[1]

Purpose. In a previous investigation it was demonstrated that circulating antibodies to a 66-kDa corneal epithelial antigen (BCEA-A) are associated with peripheral ulcerative keratitis (PUK) in patients with Wegener's granulomatosis (WG). The aim of this study was to identify BCEA-A.

Methods. The 66-kDa antigen was purified from a bovine corneal epithelial protein extract, using DE52 ion exchange chromatography. Purified protein was used to raise rabbit polyclonal antibodies. These antibodies were used to screen a bovine corneal epithelial cDNA expression library. Positive clones were purified and sequenced. Clones were identified by DNA sequence homology searches of the GenBank DNA database.

Results. A cDNA clone that demonstrated strong binding to both the rabbit polyclonal antibody and patient sera, showed 85% homology to rabbit cytokeratin 3 (K3). K3 is a basic cytokeratin specific to corneal epithelium. No bovine DNA sequence for K3 is available. However, bovine K3 is larger than rabbit K3, with a molecular weight of 66 kDa. Immunofluorescence using both patient sera and the rabbit antibody demonstrated a cytoplasmic binding pattern on human corneal epithelium.

Conclusions. This evidence suggests that the 66-kDa autoantigen (BCEA-A) associated with PUK in WG is cytokeratin 3, and this may form the basis of a diagnostic/prognostic test. (*Invest Ophthalmol Vis Sci.* 1999;40:2147–2151)

Wegener's granulomatosis (WG) is a rare inflammatory disease of unknown etiology that is characterized by vasculitis of the upper and lower respiratory tract, often in combination with glomerulonephritis. WG also can affect any other organ system, including the skin, eye, heart, nervous system, and gastrointestinal tract.[1] Early diagnosis of WG is difficult, but if diagnosed and treated promptly with immunosuppressive therapy and corticosteroids, the prognosis is much improved. Up to 90% of patients have circulating anti-neutrophil cytoplasmic antibodies.[2] The presence of these antibodies is commonly used as a diagnostic marker for this condition.[3]

Ophthalmic involvement may be present in up to 58% of WG cases. Moreover, in some cases ocular manifestations may be the major symptom or presenting feature of the disease. Although circulating anti-neutrophil cytoplasmic antibodies (usually anti–proteinase 3 antibodies) are a sensitive and specific marker for WG-associated scleritis[4] and are used in the early evaluation of patients, not all WG patients carry anti–proteinase 3 antibodies, particularly in early stages or limited presentation of the disease. In such cases, correct diagnosis and treatment may be delayed. Additional disease markers would, therefore, be a useful in the diagnostic procedure, helping to differentiate between ophthalmic manifestations of WG and other corneal inflammatory conditions with an autoimmune background.

We have previously demonstrated the presence of autoantibodies to a corneal protein of 66 kDa (BCEA-A) in WG with and without peripheral ulcerative keratitis (PUK).[5] In this study, we have purified BCEA-A and used molecular techniques to identify it as cytokeratin 3.

Methods

Methods of securing human and animal tissues complied with the National Institutes of Health Guidelines on the Care and Use of Animals in Research, the Declaration of Helsinki, and the ARVO Statement for the Use of Animals in Ophthalmic and Vision Research.

DE-52 Purification of BCEA-A

Corneal epithelium was scraped from the central region of bovine corneas. Three hundred milligrams of tissue collected from 20 eyes was homogenized in 5 ml of 1 M NaCl, 40 mM Tris/HCl, pH 7.8, containing 1 μl 10 mM phenylmethylsulfonyl fluoride. The homogenized extract then was centrifuged at 20,000g for 30 minutes. The supernatant was dialyzed against distilled water, followed by 20 mM Tris/HCl, pH 8.0, for 48 hours. The concentration of the protein was estimated by spectrophotometer at a wavelength of 280 nm. The integrity of the corneal extract was assessed by sodium dodecyl sulfate–polyacrylamide gel electrophoresis (SDS-PAGE) and Coomassie Blue staining to ensure that the proteins were not degraded. The soluble corneal extract was dialyzed into 0.05 M NaCl, 20 mM Tris/HCl, pH 7.8, and diluted to a protein concentration of 29 mg/ml in the same buffer. Five milliliters of the extract was loaded on to a DE-52 column. Unbound proteins were eluted from the column with 0.05 M NaCl, 20 mM Tris/HCl, pH 7.8. The resulting fraction was dialyzed into 20 mM Tris/HCl, pH 7.8, analyzed by SDS-PAGE, and immunoblotted with patient sera containing antibodies to BCEA-A.

SDS-PAGE and Immunoblotting

Protein from tissue extracts or antigen-enriched protein preparations were separated by SDS-PAGE and immunoblotted by standard techniques.[5]

Production of Rabbit Polyclonal Antibodies to BCEA-A

A BCEA-A–enriched extract was separated by SDS-PAGE and electroblotted onto a pure nitrocellulose membrane. The mem-

From the [1]Musculoskeletal Research Group, [2]University Department of Ophthalmology, and [3]ARC ERU, University of Manchester, and Central Manchester Health Care NHS Trust, Manchester, United Kingdom.

Supported by The Arthritis and Rheumatism Council.

Submitted for publication November 24, 1998; revised March 1, 1999; accepted March 23, 1999.

Proprietary interest category: N.

Reprint requests: M. Chantal Hillarby, Department of Rheumatology, Stopford Building, University of Manchester, Oxford Road, Manchester M13 9PT, UK.

brane was stained with Ponceau S to identify the relevant band. The identified protein band was excised from the membrane and used to raise polyclonal antibodies as described previously.[5]

RNA Extraction

Bovine corneal epithelium was powdered in liquid nitrogen and taken up in RNAzolB (Biogenesis, Poole, UK). Total RNA was purified according to the manufacturer's instructions.

cDNA Library Preparation and Screening

A cDNA expression library was made from bovine corneal epithelial mRNA in the Uni-ZAP-XR lambda vector (Stratagene, Amsterdam, The Netherlands) according to the manufacturers instructions. Briefly, cDNA was synthesized by reverse transcription using a polyT primer containing a *Xho*I restriction site at the 3′ end. *Eco*RI adapters were ligated to the two blunt termini, followed by a double digestion with *Xho*I/*Eco*RI. The resulting product was directionally cloned into the *Eco*RI/*Xho*I site of Uni-ZAP-XR vector. The resulting library contained 2×10^8 recombinant clones. The library was transfected into 200 μl of *Escherichia coli* XL-1 MRF′ cells, and 5 NZY agar plates, each containing 50,000 clones, were prepared for immunoscreening with the rabbit polyclonal BCEA-A antibodies. The antisera was diluted 1:2000 and preincubated with 12 mg/ml *E. coli* lysate prior to the library screening. Immunoscreening was carried out according to the Stratagene protocol. Positive clones were purified by secondary and tertiary screening.

DNA Sequencing

Pure clones were grown up, and phage DNA was extracted using phage DNA extraction columns according to the manufacturer's instructions (Qiagen, Crawley, UK). The size of inserts was measured on agarose gels after polymerase chain reaction amplification, using primers specific to the T3 (5′AAT TAA CCC TCA CTA AAG GG3′) and T7 (5′GTA ATA CGA CTC ACT ATA GGG C3′) binding sites. Samples were amplified for 40 cycles of 45 seconds at 94°C, 45 seconds at 60°C, and 80 seconds at 72°C. PCR products were cloned into the TA cloning vector (Invitrogen, Groningen, The Netherlands) according to manufacturer instructions. Plasmids containing inserts of the correct size were purified using Qiagen columns. Inserts were sequenced directly by cycle sequencing (BIG dye primer kit; Perkin Elmer, Warrington, UK) using M13 forward (5′GTA AAA CGA CGG CCA G3′) and M13 reverse (5′CAG GAA ACA GCT ATG AC3′) primers. Sequenced samples were run on a Perkin Elmer 377 automated DNA sequencer. Sequences obtained were used in DNA homology searches of the GenBank DNA databases using FastA.

Tissue Localization of BCEA-A by Immunofluorescence

Fresh human eyes that were unsuitable for corneal transplant were obtained from the Manchester Eye Bank and stored in a moist chamber with a balanced salt solution until the sample was processed. A corneoscleral disc was removed, using a trephine and scissors. The disc was then cut into blocks of approximately 2×10 mm, ensuring that the limbus was included. Other human tissues including esophagus, oral mucosa, liver, skin, lungs, and kidney were obtained postmortem, frozen, and cut into 5-μm sections. The tissue was snap frozen in liquid nitrogen–cooled isopentane and mounted in OCT compound. BCEA-A expression was localized in these tissues as described previously.[5]

Results

Tissue Localization of BCEA-A

Frozen sections of normal human corneas were used as the substrate in indirect immunofluorescence. The rabbit anti–BCEA-A antibodies detected antigen in human corneal epithelium showing a cytoplasmic binding pattern (Fig. 1). There was no binding to the underlying sections of cornea, i.e., Bowman's membrane, stroma, Descemet's membrane, or endothelium.

Frozen sections of normal human tissues also were used as a substrate for rabbit anti–BCEA-A antibody binding. The selected tissues included kidney, lung, liver, and skin, which are often involved in WG. The other tissues, intestine and esophagus, have a squamous epithelial layer similar to the epithelial layer of the eye. The anti–BCEA-A antibody bound only the epidermal layer of the skin, showing a cytoplasmic binding pattern, similar to the binding seen in the corneal epithelium (Fig. 1).

Identification of BCEA-A

A bovine corneal epithelial Uni-ZAP-XR lambda expression library was produced and 1×10^5 recombinant clones were screened with rabbit anti–BCEA-A antibodies. One clone (A10) was identified as positive. The rabbit antibodies were not purified for their antigen specificity; therefore, it was possible that the antibodies, which recognized clone A10, were different from those that recognize BCEA-A. Antibodies bound to A10 were eluted from the tertiary screening filter and used to probe a western blot of BCEA-A–enriched protein extract. The eluted antibodies bound to a 66-kDa band.

The 550-bp insert in clone A10 was sequenced, and a DNA homology search revealed strong homology with rabbit cytokeratin 3 and human keratin 2 (Table 1). The DNA sequence of A10 was translated into a putative amino acid sequence, and protein homology searches were performed. The results from these searches confirmed the strong homology between clone A10 and basic cytokeratins 3 and 2 (Table 1, Fig. 2).

To confirm the identity of BCEA-A as keratin, a human epidermal keratin extract (ICN) containing both basic and acidic keratins was probed with both human sera and rabbit anti–BCEA-A antibodies. The keratin preparation was resolved by SDS-PAGE along with a BCEA-A–enriched protein extract. Immunoblotting with rabbit anti–BCEA-A antibodies and human serum known to carry anti–BCEA-A antibodies revealed binding to a band slightly above 66 kDa (Fig. 3).

Discussion

We previously reported the association of antibodies to a basic 66-kDa corneal epithelial–derived antigen (BCEA-A) and PUK-associated WG.[5] To further characterize this antigen, rabbit polyclonal antibodies were raised and used to localize CEA-A by indirect immunofluorescence, which demonstrated that BCEA-A is expressed in the epithelium of human cornea and in human skin epidermis. A bovine corneal epithelial cDNA library was screened with the rabbit anti–BCEA-A antibodies and

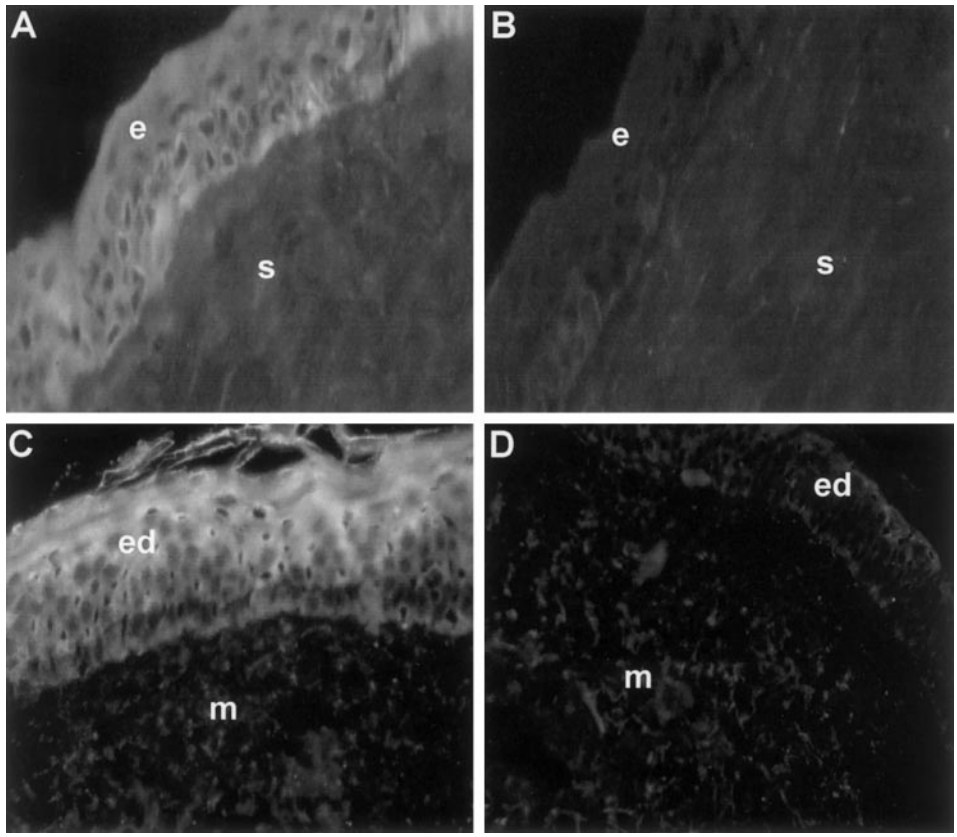

FIGURE 1. Detection of BCEA-A in noncorneal tissues. Several human tissues, including cornea (**A**, **C**), kidney and skin (**B**, **D**), lung, esophagus, intestine, and liver, were screened with rabbit anti–BCEA-A sera. BCEA-A was only detected in the cornea (**A**) and skin (**C**) sections. No positive staining was detected when the secondary antibodies were used alone (**B**, **D**). e, epithelium; s, stroma; ed, epidermis; m, dermis.

a positive clone was isolated, purified, and sequenced. The clone showed 85% DNA homology with a rabbit corneal–specific cytokeratin. This as well as other indirect evidence indicates that BCEA-A is cytokeratin 3.

The clone A10, identified by antibody binding, showed 85% DNA homology and 87.9% amino acid homology with rabbit cytokeratin 3 (K3). The homology of the A10 clone also was compared with other members of cytokeratin family and with cytokeratins across species. The result revealed 78% amino acid homology with human skin keratin 2 (K2), and 84% homology with human K3. Neither the DNA nor the amino acid sequence of bovine K3 is available on databases. However, human and rabbit K3 sequences showed 80% amino acid homology to one another. Therefore, it is likely that the homology of 87.9% between A10 clone and rabbit K3 is due to the species differences between rabbit and bovine K3.

K3 is a member of the intermediate filament (IF) superfamily of proteins. Keratins are the major structural components of the cytoskeleton that are exclusively expressed by epithelial cell types throughout the body. K3 is a basic component in a pair with acidic cytokeratin 12 (K12); both proteins are cornea specific, and bovine K3 weighs 66 kDa.[6] These characteristics make K3 a good candidate for BCEA-A, which is corneal epithelial–specific, basic, and 66 kDa.

To further investigate the possible identity of BCEA-A as K3, a preparation of human skin epidermal keratins was immunoblotted with rabbit anti–BCEA-A antibodies and with human serum positive to BCEA-A. This preparation was chosen, in the absence of purified corneal epithelial keratin, because human K2 and K3 share 80% identity, therefore, polyclonal antibodies to K3 are likely to cross-react with K2. The experiment revealed a very strong binding of rabbit anti–BCEA-A antibodies to a spectrum of keratins present in skin epidermal preparation. It also showed pronounced binding of human serum antibodies to a band positioned slightly higher than 66 kDa (human K2 is 67 kDa) in the same preparation. Both types

TABLE 1. Homology between the cDNA and Putative Amino Acid Sequence of Clone A10 and Basic Keratin Sequences

	DNA		Amino Acid	
Comparison	**Position (bp)**	**Homology (%)**	**Position (aa)**	**Homology (%)**
Clone A10 vs rabbit K3*†	432–670,1600–1769	85	116–238	85
Clone A10 vs human K3‡			118–253	84
Clone A10 vs human K2§‖	372–907	79	109–236	78
Human K3‡ vs rabbit K3†				80

Sequence numbers: *GenBank S65740; †Pir S42629; ‡SwissProt P12035; §GenBank 99063; ‖SwissProt Q01546.

```
Clone A10 G F G G A G G F G G  A G A F G G L G G F  G G P G G F G - - -  - - - - - - - - - -  P G G F G P G G F P
Rabbit K3 G F G G - - G F G G  A G A F G G A G G F  G G A G G F G G P G  - - - - - - - - - -  - G F G G P G G F P
Human K3 G F G G A G G F G G  A G G F G G A G G F  G G P G G F G G S G  G F G G P G S L G S  P G G F A P G G F P
Human K2 G R G V G S G F G G  A G G F G G A G G F  G G P G V F G G P G  S F G G P G - - - -  - - G F G P G G F P

Clone A10 G G I Q E V T V N Q  S L L Q P L S V E I  D P Q I G Q V K T Q  E R E Q I K T L N N  K F A S F I D K V R
Rabbit K3 G G I Q E V T V N Q  S L L Q P L N V E I  D P Q I G Q V R A Q  E R E Q I K T L N N  K F A S F I D K V R
Human K3 G G I Q E V T T N Q  S L L Q P L K V E T  D P Q I G Q V K A Q  E R E Q I K T L N N  K F A S F I D K V R
Human K2 G G I Q E V I V N Q  S L L Q P L N V E I  D P Q I G Q V K A Q  E R E Q I K T L N N  K F A S F I D K V R

Clone A10 F L E Q Q N K V L E  T K W S L L Q Q Q G  T H P I K G T N N L  E P L F E N
Rabbit K3 F L E Q Q N K V L E  T K W E L L Q R Q G  P N S V T G T N N L  E P L F E N
Human K3 F L E Q Q N K V L E  T K W N L L Q Q Q G  T S S I S G T N N L  E P L F E N
Human K2 F L E Q Q N K V L E  T K W E L L Q Q Q T  T G S - - G P S S L  E P C F E S
```

Figure 2. Amino acid sequence alignment of clone A10 with rabbit and human keratin. The putative amino acid sequence of clone A10 compared to rabbit and human keratin 3 and human keratin 2. Areas of nonhomology are *shaded.*

of antibody also recognized a 66-kDa band in both nonpurified extract and BCEA-A–enriched extract. This result strongly suggests that the original antigen against which anti–BCEA-A antibodies were raised is K3.

To further confirm the identity of BCEA-A as K3, immunohistochemistry was used to localize the antigen within human skin and cornea. In a study of K3 expression in rabbit cornea, using the highly specific monoclonal antibody AE5, it has been demonstrated that K3 is localized to corneal epithelium and the suprabasal layer of the limbus.[7] The localization of BCEA-A using indirect immunofluorescence on frozen corneal sections showed that rabbit and human antibodies recognize an antigen in both the corneal and limbal part of the epithelium, in keeping with the expected pattern for K3. The cross-reactivity of anti BCEA-A antibodies with skin epidermal keratins has been confirmed by indirect immunofluorescence (IIF) on frozen human skin sections. The antibody binding on these sections was limited to the epidermal layer above the basal layer of the human skin, where K2 (the skin equivalent of K3) is localized.[8] Moreover, the homology search demonstrated that K2 has the highest amino acid and DNA homology to K3 and clone A10, in comparison with other human keratins. This implies that K2 is a likely target for cross-reacting anti–BCEA-A antibodies, which may explain the lack of binding of anti–BCEA-A antibodies to other tissues, such as intestine and esophagus, with different type of epithelium containing basic type keratins of much lower homology to K3, e.g., K4 (esophageal equivalent of K3), which shows only 68% homology with clone A10 and K3. The above results strongly suggest that the target antigen for anti–BCEA-A antibodies in the cornea is K3.

Autoantibodies against constituents of the cytoskeleton have been reported and investigated by a number of groups.

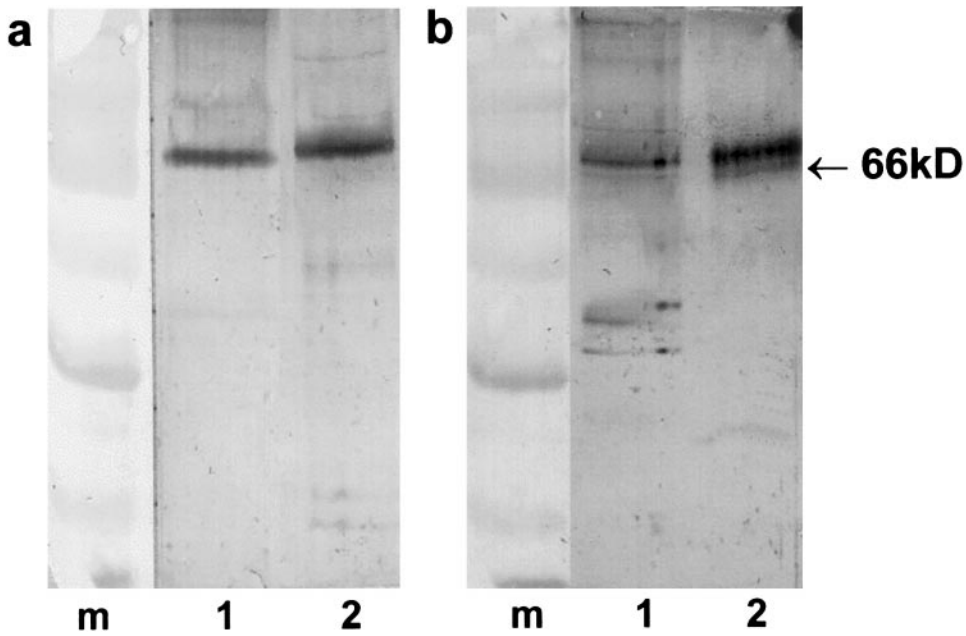

Figure 3. Binding of rabbit and human anti-BCEA-A antibodies to human skin epidermal keratin. BCEA-A enriched protein extract (1) and human epidermal keratins (ICN) (2) were separated by SDS-PAGE, blotted, and probed with rabbit anti–BCEA-A antibodies (**a**) and patient sera (**b**). m, moleculer weight markers.

The best characterized are anti-filaggrin antibodies,[9] which are specific for RA and often appear before clinical onset of the disease.[10] However, to the date there have been no reports of anti-cytoskeleton antibodies present in primary systemic vasculitis.

We previously have demonstrated that a high percentage of WG patients, especially those with eye complications, have antibodies to a corneal protein (BCEA-A). In this study we identified this protein as cytokeratin 3. Identification of disease-specific markers provides a tool for investigation into disease pathology and etiology and may also provide new diagnostic or prognostic markers. Further investigation will be required to define the role of anti-K3 antibodies in disease pathology and their suitability as diagnostic markers for WG and PUK.

Anti-K3 antibodies are present in a large proportion of WG patients, in particular those with eye complications. Even though it is unclear what the role or source of these antigens is, they may prove a valuable diagnostic marker in WG and PUK.

References

1. Leavitt RY, Fauci AS, Bloch DA, et al. The America College of Rheumatology 1990 Criteria for the Classification of Wegener's Granulomatosis. *Arthr Rheum.* 1990;33:1101–1107.
2. Kallenberg CGM, Mulder AHL, Tervaert JWC. Antineutrophil cytoplasmic antibodies—a still-growing class of autoantibodies in inflammatory disorders. *Am J Med.* 1992;93:675–682.
3. Jayne DR, Gaskin G, Pusey CD, Lockwood CM. ANCA and predictiotory relapse in systemic vasculitis. *Mon J Assoc Physicians.* 1995;88:127–133.
4. Jager MJ, Vos A, Pasmans S, Hoekzema R, Broersma L, Vandergaag R. Circulating cornea-specific antibodies in corneal disease and cornea transplantation. *Graefes Archive Clin Exp Ophthalmol.* 1994;232:82–86.
5. Reynolds I, John SL, Tullo AB, et al. Characterization of two corneal epithelium derived antigens associated with vasculitis. *Invest Ophthlmol Vis Sci.* 1998;39:2594–2601.
6. Cooper D, Sun TT. Monoclonal-antibody analysis of bovine epithelial keratins—specific pairs as defined by coexpression. *J Biol Chem.* 1986;261:4646–4654.
7. Schermer A, Galvin S, Sun TT. Differentiation-related expression of a major 64k corneal keratin in vivo and in culture suggests limbal location of corneal epithelial stem-cells. *J Cell Biol.* 1986;103:49–62.
8. Sun TT, Eichner R, Nelson WG, et al. Keratin classes—molecular markers for different types of epithelial differentiation. *J Invest Dermatol.* 1983;81:S109–S115.
9. Girbal E, Sebbag M, Gomesdaudrix V, Simon M, Vincent C, Serre G. Characterization of the rat esophagus epithelium antigens defined by the so-called antikeratin antibodies, specific for rheumatoid-arthritis. *Ann Rheum Dis.* 1993;52:749–757.
10. Cordonnier C, Meyer O, Palazzo E, et al. Diagnostic-value of anti-ra33 antibody, antikeratin antibody, antiperinuclear factor and antinuclear antibody in early rheumatoid-arthritis—comparison with rheumatoid-factor. *Br J Rheumatol.* 1996;35:620–624.

Conversion of Lens Slit Lamp Photographs into Physical Light-Scattering Units

Thomas J. T. P. van den Berg and Joris C. Coppens

Purpose. To derive from lens slit lamp photographs by means of densitometry the physically defined quantity for light scattering (the Rayleigh ratio) and to expand the use of the Lens Opacity Classification System (LOCS III) to include clear lenses and also to calibrate the LOCS III Nuclear Opacity (NO) score in physical terms.

Methods. Series of slit lamp photographs were taken from 38 eyes from 29 subjects (age range 18 to 84 years old) including cataracts, for 0.1- and 0.2-mm slit width, using 200 ASA and 1600 ASA film speed (Kodak professional; Eastman Kodak, Rochester, NY) and different flash settings with a Topcon SL-6E (12 slit/speed/flash combinations; Paramus, NJ). Additionally 19 eyes were photographed with a Zeiss 40 SL/P (8 slit/speed/flash combinations; Carl Zeiss, Thornwood, NY). A calibrated suspension of latex spheres also was photographed at the same 20 conditions. Densitometry was performed on the nuclear area of all photographs including the LOCS III standards, using a photometrically corrected photocell. Slit width and flash intensity settings were photometrically calibrated. All eyes and the suspension were digitally "photographed" with the EAS-1000 (Nidek, Gamagori, Japan) Scheimpflug system.

Results. For each eye and the suspension, the series of 20 or 12 densities, corresponding to a range of about 1 log unit in the amount of light used, proved to follow closely a course common to all eyes (the two film characteristics), apart from a shift in the amount of light (because of the differences in light back scattering).

Conclusions. From normal slit lamp photographs, the physical quantity for light (back) scattering can be derived using transformation graphs derived in this study. The LOCS III NO score also can be used for clear lenses and translated into physical units. In this way, slit lamp photography can be used better for more precise studies, provided some minimal calibration of the photograph slit lamp. (*Invest Ophthalmol Vis Sci.* 1999;40:2151–2157)

Slit lamp observation, direct or photographic, is still the major way to assess the condition of the optical media of the patient's eye. Although the slit lamp is unsurpassed for visualization of lens details, it has long been realized that the observation cannot be used directly for comparative research, especially in epidemiologic studies. Cataract classification systems were developed, i.e., methods to transform the subjective slit lamp observation to semi-quantitative data.[1–4] Slit

From the Netherlands Ophthalmological Research Institute and AMC/Department of Medical Physics, Amsterdam, The Netherlands.

Supported by the Technology Foundation (STW).

Submitted for publication October 13, 1998; revised February 10, 1999; accepted March 25, 1999.

Proprietary interest category: N.

Reprint requests: Thomas J. T. P. van den Berg, AMC/Dept. Med. Physics, PO Box 22660, 1100 DD Amsterdam, The Netherlands.

Table 1. Parameters of the Photographs Made

	Topcon SL-6E				Zeiss 40 SL/P			
Film Speed (ASA):	200		1600		200		1600	
Slit width (mm):	0.1	0.2	0.1	0.2	0.1	0.2	0.1	0.2
Flash setting								
2	−	−	−	+	−	−	−	+
3	−	+	+	+	−	+	+	+
4	+	+	+	+	+	+	+	+
5	+	+	+	+	*	*	*	*

* Not present at this instrument.

lamp observation rests on light that is scattered (or reflected) backwards. This backscattered light can also be measured with photosensitive devices giving objective and quantitative data.[5–12] However, these instruments have not (yet) pushed aside the slit lamp biomicroscope.

All the above methods use the backscattered light, but results are presented in more or less arbitrary units, different between the different methods. A physical definition of light scattering is given by the so-called Rayleigh ratio *R*. It would be valuable if such a well-defined and generally applicable unit could be used easily in lens research. This would aid, e.g., in the comparison between epidemiologic studies or for in vivo versus in vitro studies. Because of the dominance of the normal slit lamp, we studied whether this instrument can be used to estimate *R* in a simple way.

Two approaches were evaluated, photographic and direct observation at the slit lamp. Photographic information can be transformed to quantitative data by densitometry. With careful calibration of the photographic procedure and the use of a backscattering standard, a direct relationship can be established between photograph density and *R*. However, to eventually avoid the need for densitometry, a transformation from subjective cataract score to *R* also was developed. As the scoring system, LOCS III for nuclear opacity (NO) was used.[4] In this system, a direct slit lamp picture or a photograph is compared by eye to five standard photographs with different grades of nuclear opacity, numbered 1 to 5. The densities of these five photographs also were measured and transformed to *R*. The NO score of a patient's lens, e.g., 3.6 (one decimal place by visual interpolation), can then be transformed to *R*. Both transformation techniques, densitometry-based as well as LOCS III–based, were tested against independent assessments of *R* on the same lenses.

Methods

Series of slit lamp photographs were taken in two groups: (1) from 19 eyes from 19 subjects (age range 18 to 64 years old), each photograph once repeated, and (2) from 19 eyes from 10 subjects (age range 55 to 84 years old, from a cataract clinic, some with nuclear cataract), without repetitions. For all eyes, 12 photographs were made with 0.1- and 0.2-mm slit width, using 200 ASA and 1600 ASA film speed (Kodak professional; Eastman Kodak, Rochester, NY), and different flash settings (see Table 1) with a Topcon SL-6E (12 slit/speed/flash combinations; Topcon, Paramus, NJ). Additionally, the first group of 19 eyes was photographed with a Zeiss 40 SL/P, also with 0.1- and 0.2-mm slit width, using 200 ASA and 1600 ASA film speed (8 slit/speed/flash combinations; Carl Zeiss, Thornwood, NY; see Table 1). The light sources were the standard xenon-filled flash tubes, used in these instruments, with no color filters interposed. A calibrated suspension of latex spheres was photographed at the same 20 conditions. The suspension was contained in an artificial eye, the "cornea" consisting of a zero-diopter, 8-mm-radius contact lens. Readings were taken at 2 mm behind the "cornea." Photographic magnification was 2.2 for the Topcon and 1.8 for the Zeiss camera. This difference causes in itself a difference in film exposure of a factor $(2.2/1.8)^2 = 1.5$ (0.17 log units) higher exposure, corresponding to lower magnification (the Zeiss camera). The films were developed by a certified professional photograph laboratory (Q-laboratory). Standard procedures in such a laboratory include developing a trial film every morning and evening and checking it densitometrically, and once a week Kodak checks the film. The photographic procedures were according to and including the set of conditions of the LOCS system (200 ASA, 0.2 mm, etc.).

Densitometry on the nuclear area of all photographs including the LOCS III standards (positive color transparencies of the standard 2.4 × 3.6-cm size) was performed using a photometrically corrected photocell. A circular diaphragm in front of the photocell was adjusted to cover the full depth of the nucleus, defined according to other densitometric studies.[4,13] Slit width and flash intensity settings were calibrated with the help of a photometrically corrected photocell, placed at the same position as the patient's eye, which was large enough to collect all light. All eyes and the suspension also were digitally "photographed" with the EAS-1000 Scheimpflug system (Nidek, Gamagori, Japan).

As physical unit for the light-scattering property of scattering materials, the so-called Rayleigh ratio is used:

$$\text{Rayleigh ratio} = R(\theta) = I(\theta) \div E*V, \quad \text{or} \quad I(\theta) = R(\theta)*E*V,$$

with $I(\theta)$ the amount of light scattered per unit solid angle in W/steradian by a volume of scatterer V in m^3 illuminated by incident light E in W/m^2. In the present study, $I(\theta)$, where $\theta = 135°$, is proportional to the amount of light collected by the reception aperture of the slit lamp microscope, part of which is projected on the photographic film. The resulting light density on the film is proportional to 1/magnification.[2] $I(\theta)$ is proportional on the other hand to E, which is controlled by the

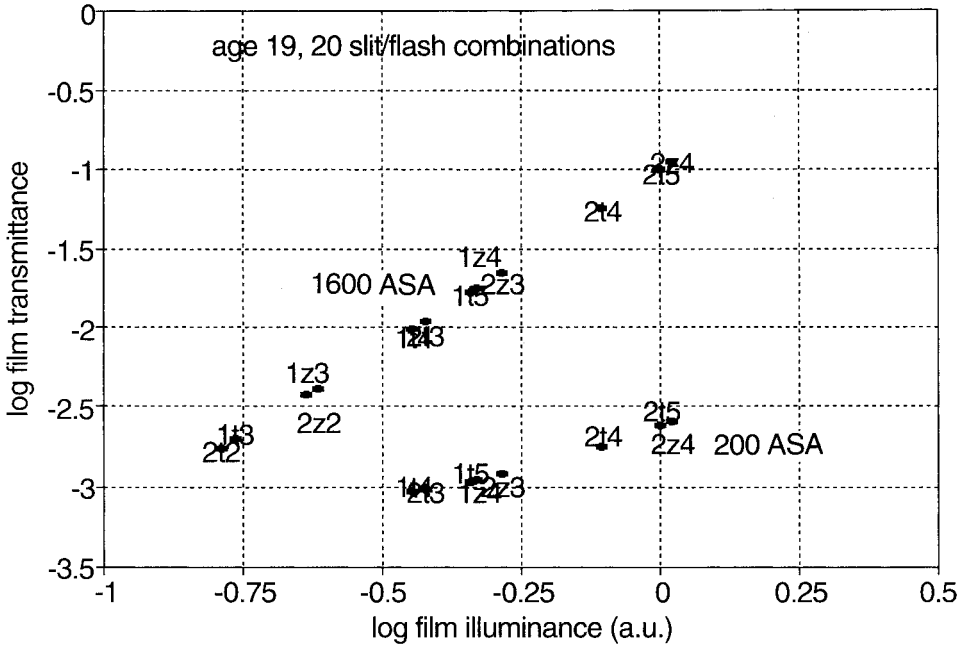

FIGURE 1. Densitometric values using a photometrically corrected photocell of the nucleus in slit lamp photographs from a 19-year-old subject for different slit/flash combinations. The amount of light delivered by the different slit/flash combinations was photometrically calibrated (*horizontal axis*). The codes denote slit/slit lamp/flash, e.g., 2t4 denotes 0.2-mm slit/Topcon/flash no. 4. The *symbols* are the results of a fit of a function describing the film characteristic.

flash setting on the slit lamp. In fact, instead of $I(\theta)$ and E, their integrals over the full flash duration determine film exposure. $I(\theta)$ and film exposure depend moreover on slit width, because V does. In fact, because of limited depth of focus of the slit projection system, E is not constant over lens depth. However, because slit width is small, only the total E over slit width (in the focal plane $E \times$ slit width), in combination with the surface of the illuminated cross section instead of V, need be considered. The maximal flash was larger with the Zeiss instrument, but the reception aperture was smaller (larger depth of focus), resulting in about equal film exposure, apart from the magnification effect (factor 1.5).

For the suspension of latex spheres in water, at a concentration of 5×10^{-5} weight fraction and a sphere radius of 98 nm, the Rayleigh ratio for unpolarized light at 135° $R(135) = 1.0\ m^{-1}\ Sr^{-1}$, more or less constant between 450 and 650 nm. This was measured separately using a radiometric setup described earlier.[14–16] On the basis of the mentioned parameter values and a refractive index of about 1.58, slightly depending on wavelength, the experimental result was found to be in keeping with well-established theory, using the so called Rayleigh–Gans approximation.[17] It must be noted that these spheres are intermediary between the well-known small particle Rayleigh domain (scattering proportional to wavelength^{-4}) and the large particle domain with deep local minima in scattering as a function of angle, first appearing on the small wavelength side. For the present suspension, e.g., at precisely 500 nm $R(135) = 0.97$ and at

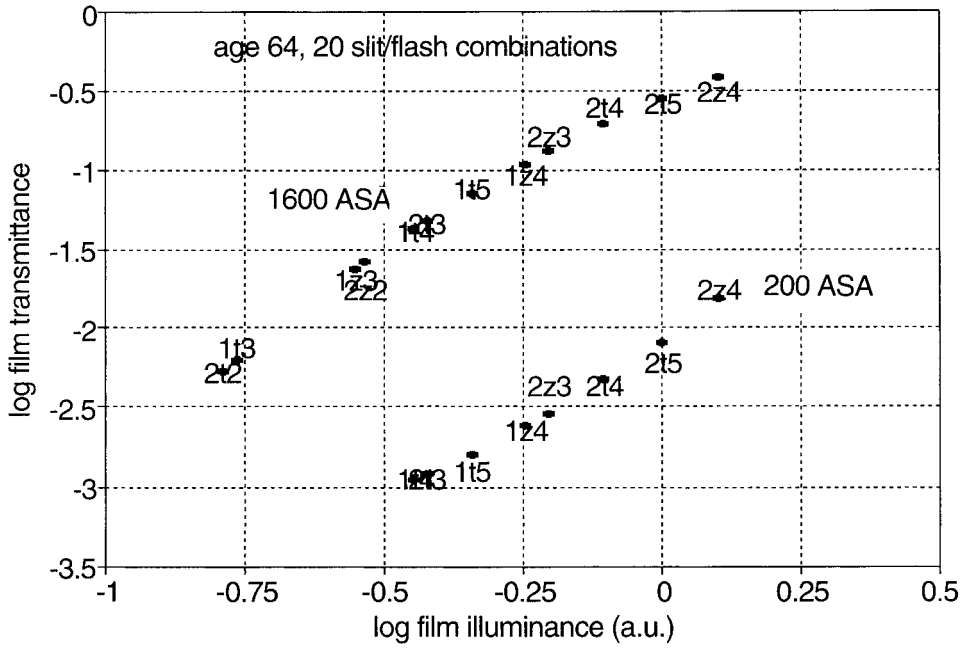

FIGURE 2. Densitometric values using a photometrically corrected photocell of the nucleus in slit lamp photographs from a 64-year-old subject for different slit/flash combinations. The amount of light delivered by the different slit/flash combinations was photometrically calibrated (*horizontal axis*). The codes denote slit/slit lamp/flash, e.g., 2t4 denotes 0.2-mm slit/Topcon/flash no. 4. The *symbols* are the results of a fit of a function describing the film characteristic.

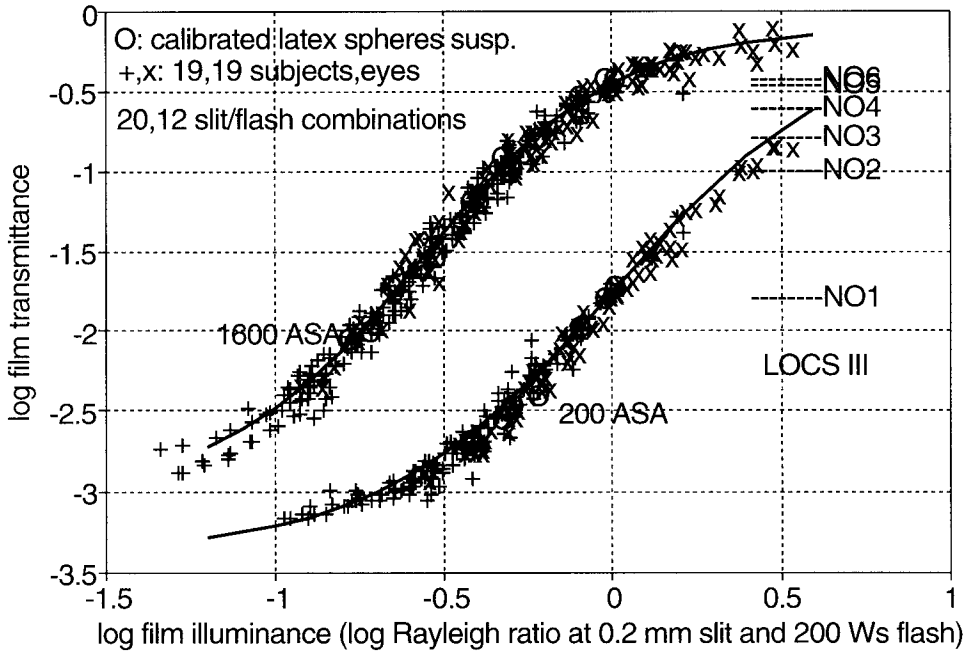

FIGURE 3. The combined data for all subjects (exemplified in Figs. 1, 2) show a common course (the two film characteristics). The 20 plotted values for a suspension of latex spheres (*circles*) are calibrated to yield absolute values for the *horizontal axis* (Rayleigh ratios in m^{-1} Sr^{-1}). *Continuous lines* show the fitted functions for the two film characteristics. To the *right*, the densities are indicated of the LOCS III NO standards NO1 through NO6 (−1.76, −0.97, −0.76, −0.58, −0.43, and −0.39, respectively).

600 nm $R(135) = 1.03$. Throughout this article, Briggsian logarithms (base 10) are used.

RESULTS

Figures 1 and 2 show examples of the relation between log film transmittance (= minus photograph density) and relative film illuminance for a 19-year-old subject and a 64-year-old subject, respectively. To clarify these figures, it must be noted that film characteristics generally are described by log(film transmittance) = function[log(I_{film})]. For any camera, film illuminance $I_{film} = k \cdot R \cdot I_{source}$, where I_{source} is the light intensity incident on the sample, R is the back scattering strength of the sample, and k is a constant depending on the camera and its settings. So, log(film transmittance) = function [log(k) + log(R) + log(I_{source})]. Thus, plots of log(film transmittance) versus [log(k) + log(I_{source})] for samples having different scattering strengths should have the same shape, but they are shifted along the horizontal axis according to their log(R) values. The dependence on k and I_{source} is combined in "relative film illuminance," which is plotted along the horizontal axis and is calculated using the above calibration factors for the two instruments (a factor 1.5 difference due to magnification), the two slit widths (factor 2 difference), and the seven different flash settings. All these factors were combined to arrive at a value for film illuminance relative to the condition (Topcon, 200-W flash, 0.2-mm slit width). The curves for the two subjects show the same shape, only shifted horizontally because the nucleus of the older lens scatters a larger proportion of the incident light backwards.

Figure 3 shows the data of all subjects superimposed, after individual adjustment for the horizontal shift, based on the least squares criterion. In compliance with the correspondence between Figures 1 and 2, this figure shows that the curves for all subjects follow a common course, viz. the two film characteristics. The circles give the data for the latex spheres suspension with known Rayleigh ratio R. The horizontal axis was chosen such that the data point (Topcon, 200-W flash, 0.2-mm slit width) lies at the correct R. The drawn lines are four-parameter fits for the four-parameter logistic literature model for film characteristics.[18] For 200 ASA: log film transmittance = $-3.38 + 3.27/(1 + 10^{-1.25(\log R - 0.01)})$. For 1600 ASA: log film transmittance = $-3.01 + 2.90/(1 + 10^{-1.52(\log R + 0.57)})$. These parameters were adjusted simultaneously with the above-mentioned horizontal shifts (one for each lens), on the basis of the least squares criterion. It must be noted that the film characteristics themselves could have been estimated independently, using only the latex suspension or other samples of backscattering material. Instead, we chose to use the available dataset, because one may expect that using much data gives better estimates for the film characteristics.

Also indicated in Figure 3 are the findings for log film transmittance of the LOCS III standards NO1 through NO6. For research that uses precisely the LOCS III settings (200 ASA, 0.2-mm slit width, etc.), the following are the respective log R values for the NO standards that can be read from this figure: 0.00, 0.37, 0.49, 0.62, 0.77, and 0.82. If one would only change the use of film to 1600 ASA, the values are, respectively, −0.65, −0.33, −0.22, −0.11, 0.01, and 0.06. A warning must be placed here that the LOCS grades presented in this article no longer directly grade the respective lenses. To be more precise, the LOCS system grades *images* of the lenses. Because in the original LOCS system the images are produced identically to the way that the LOCS standards themselves are produced, there is a one-to-one relationship between grades and lenses. In the present study, the images may be produced in different ways to accommodate a broader range of applications, especially a broader range of intrinsic lens-scattering efficiencies. So, the LOCS grades must be interpreted, *depending* on the way the images are produced.

Figure 3 could be used directly to derive R from log film transmittance of a slit lamp photograph made with the Topcon at 200-W flash and 0.2-mm slit width. Because it is more customary to have the independent variable (log film

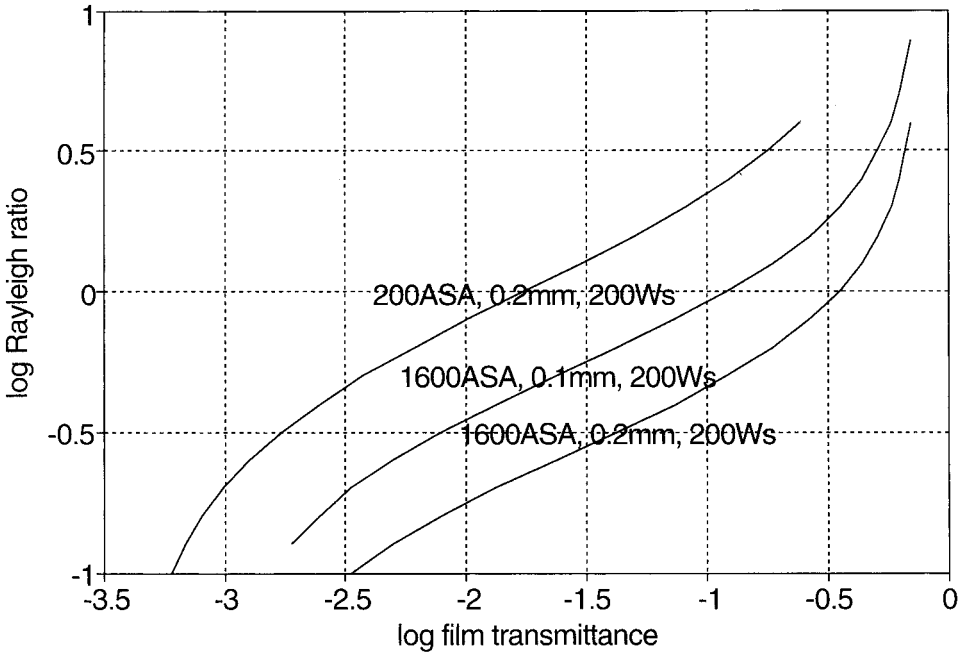

FIGURE 4. Calibration curves to derive log Raleigh ratio (*vertical*) from film density (*horizontal*). The curves are slightly different for the two film speeds. For either film speed, the curves for different flash/slit width settings differ only in vertical position. In the example given for 1600 ASA, the 0.1-mm curve is plotted at precisely a factor of 2 (0.3 log unit) higher than the 0.2-mm curve.

transmittance) horizontally, in Figure 4 the *x*- and *y*-axis are exchanged, but the same model lines are drawn. For other flash or slit width settings, a correction for the difference in light content must be made, which is a simple shift because of the logarithmic *R* axes. Figure 4 gives as an example the line for 1600 ASA, 0.1-mm, and 200 W. Figure 4 is the calibration graph in case log film transmittance (optical density) is available.

If, however, scoring with the LOCS III system is used, another calibration graph is needed (Fig. 5). Also, this graph is derived from Figure 3. For each of the 6 NO standards the intersections of log film transmittance with the two film characteristics gives the *R* values for 200-W flash and 0.2-mm slit width. These values are plotted in Figure 5. For other flash or slit width settings, the film characteristics also must be shifted. Figure 5 gives as example the line for 1600 ASA, 0.1-mm, and 200 W. Each potential calibration line in Figure 5 can be derived graphically from Figure 3 (if needed, after the appropriate horizontal shift) or numerically, using the above formulas for the two film characteristics and the values for log film transmittance of the LOCS III NO standards: −1.76, −0.97, −0.76, −0.58, −0.43, and −0.39.

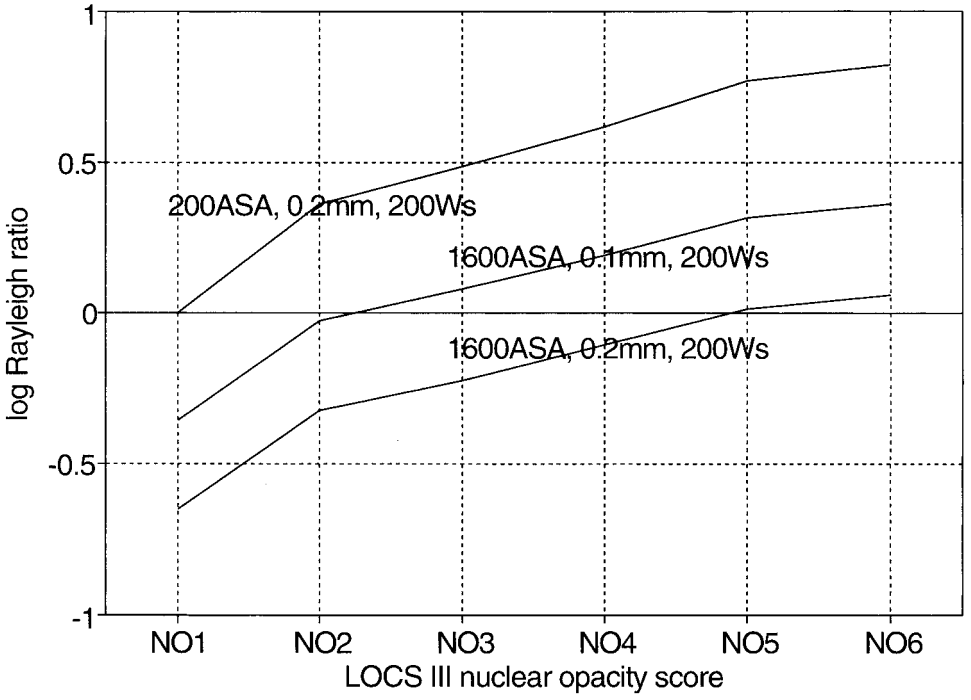

FIGURE 5. Calibration curves to derive log Raleigh ratio (*vertical*) from the LOCS III NO score (*horizontal*). The curves are slightly different for the two film speeds. For either film speed, the curves for different flash/slit width settings differ only in vertical position. In the example given for 1600 ASA, the 0.1-mm curve is plotted at precisely a factor of 2 (0.3 log unit) higher than the 0.2-mm curve.

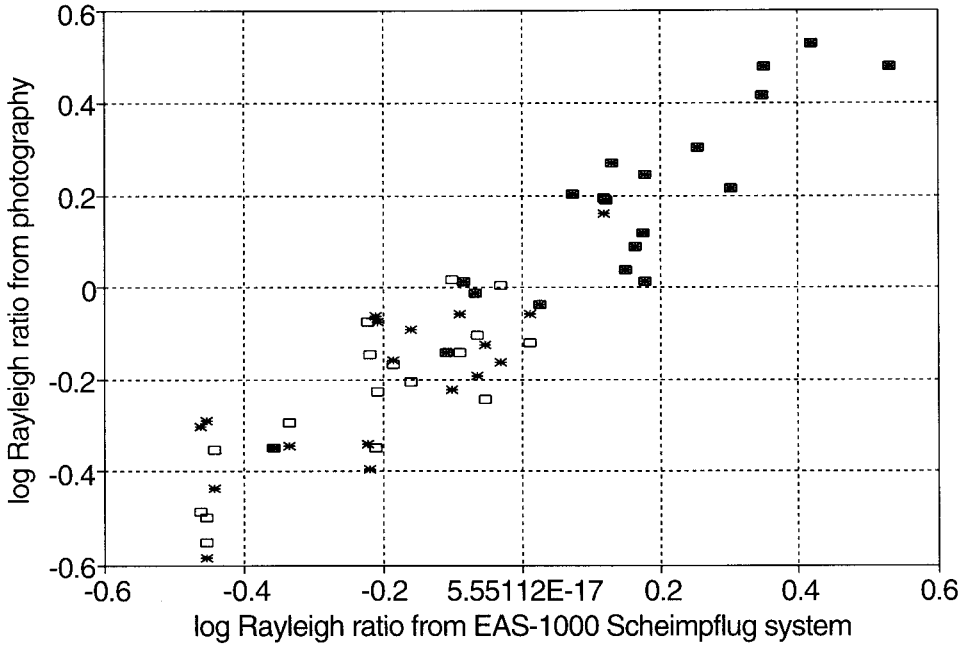

FIGURE 6. Comparison between log Rayleigh ratios obtained respectively with the present photographic/densitometric method and an independent measurement using a calibrated Scheimpflug system. One eye of 19 subjects was photographed with a Zeiss (*stars*) and a Topcon (*open squares*) slit lamp. Nineteen eyes of 10 older subjects were photographed with a Topcon slit lamp (*filled squares*).

DISCUSSION

The present study was designed to translate slit lamp photographs to physical light-scattering units, the Rayleigh ratio *R*. Densitometry on the nucleus was performed, but, of course, the relation between the densitometric values and *R* holds equally for other parts of the lens. It must be noted, however, that the observed intensity of the backscattered light can be influenced by light absorption in the lens. For younger lenses, this is of little consequence, because the lens pigments absorb predominantly below 500 nm, whereas the photometric and visual sensitivity used in this study lies predominantly above 500 nm. In older lenses, pigments may accumulate to such amounts that backscattered light from deeper layers, especially from the posterior pole, may be weakened significantly. The observed intensity of the backscattered light also can be influenced by scattering of both the incident light or the scattered light itself. These effects are, however, unimportant because only minute amounts are scattered over larger angles. Only a few percent is scattered over more than 10°.[19,14]

The outcomes of both presented methods were verified (Figs. 6, 7). Figure 6 shows a result of the densitometric approach for the same subjects as used to construct Figure 3; Scheimpflug images also were made with an EAS-1000 instrument. This instrument was calibrated, using the same

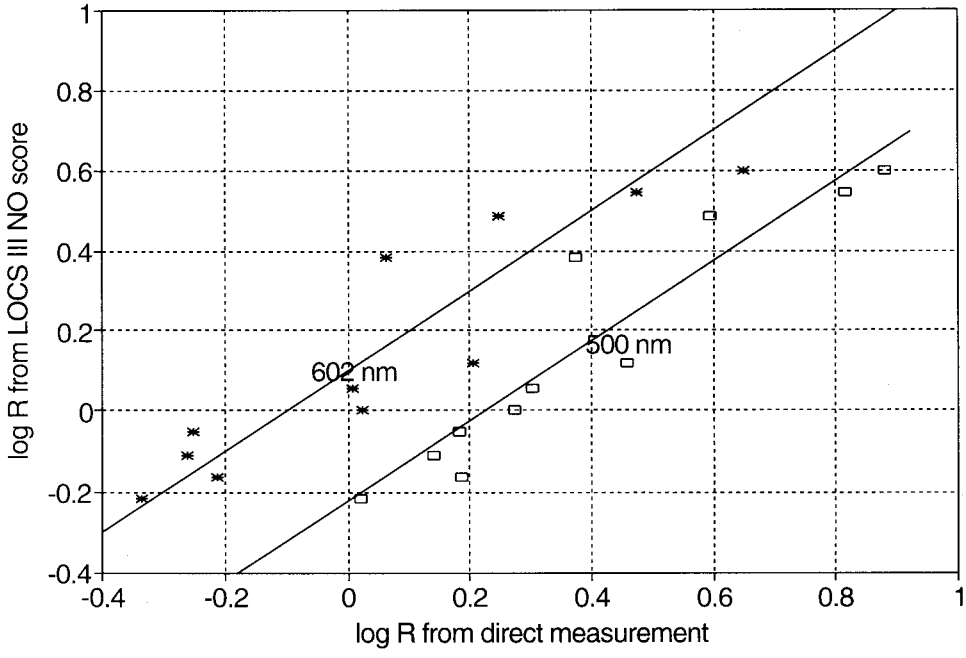

FIGURE 7. Comparison between log Rayleigh ratios obtained with the present photographic/LOCS III–based scoring system and an independent physical measurement at 500 nm (*open squares*) and at 602 nm (*stars*), respectively. The *continuous lines* represent the ideal case.

suspension of latex spheres, in terms of Rayleigh ratio. Figure 6 shows that the correspondence is close, considering that different planes are cut through the lens. The Scheimpflug instrument cuts the lens over its optical axis, and the slit lamp biomicroscope cuts the lens obliquely at 45° from its optical axis.

Figure 7 shows verification of the approach using LOCS III NO scoring. For this figure, data were used from a study on light scattering by lenses extracted from donor eyes.[14–16] Twelve lenses were photographed using 1600 ASA film speed, because these were age-normal lenses (except one lens with nuclear cataract), and scored using the LOCS III NO system. The main issue was to measure and interpret the light-scattering properties in forward as well as backward directions at wavelengths 400, 500, 602, and 700 nm. Figure 7 shows horizontally log Rayleigh ratio of the nucleus for 602 and 500 nm at 140° (40° backwards). Vertically log Rayleigh ratio is plotted as read from the present Figure 5 using the NO scores given earlier.[14] Note that the present approach involves implicitly averaging over the middle of the visual spectrum, i.e., 555 ± 50 nm. Indeed, Figure 7 shows that the values found are between those for 500 and 602 nm. The ideal correspondence is represented by the two lines, which are positioned according to the well-known wavelength^{-4} dependence of light scattering by small particles. It recently was found that this type of scattering dominates in human lenses in the relevant angular domain (around 40° or 45° backward scattering), especially in the nucleus.[16] The variability in Figure 7 is larger than in Figure 6. This can be expected because the comparison of Figure 7 involves not only different cuts through the lenses, as in Figure 6, but also other differences. NO scoring involves a subjective judgment. Moreover, the data are from a completely independent study, performed on donor lenses. Important in this study was that direct measurements on wavelength-resolved Rayleigh ratios were performed. In view of all the differences, the correspondence shown in Figure 7 seems satisfactory.

In conclusion, normal slit lamp observation and photography can be used to derive the physically defined measure for light scattering, the Rayleigh ratio, making it more suitable for comparative studies. With Figures 4 and 5 and eventually the formulas for the two film characteristics and the density values for the LOCS III NO standards, the conversion can be made directly in case proper standard procedures are followed, such as defined in the LOCS III standard. To include a wider range of applications, the LOCS III standard was extended to include using the 200-W flash tube, professional Kodak film of 200 or 1600 ASA, well-defined slit widths (0.2 or 0.1 mm), and illumination at 45° from the optical axis, along which photography is performed. Some minimal calibration of the slit lamp is highly advisable though. A good way to calibrate is to photograph with one's standard settings the latex suspension defined in the Methods section. The densitometric value of the latex spheres' photograph, using a photometric photocell, fixes the position along the horizontal axis of the curves of Figure 3 (vertically in Fig. 4). In other aspects, these curves remain the same. It would be most accurate if the photographs of the patients also are measured densitometrically in the same way. Otherwise, one would proceed to derive one's own curves of Figure 5 and to use the normal LOCS III NO scores.

References

1. Chylack LT Jr, Lee MR, Tung WH, Cheng HM. Classification of human senile cataractous change by the American Cooperative Cataract Research Group (CCRG) Method I. Instrumentation and technique. *Invest Ophthalmol Vis Sci.* 1983;24:424–431.
2. Sparrow JM. Methods of clinical cataract grading: two systems compared. *Arch Ophthalmol.* 1990;108:1209–1211.
3. Taylor HR, Lee JA, Wang F, Munoz B. A comparison of two photographic systems for grading cataract. *Invest Ophthalmol Vis Sci.* 1991;32:529–532.
4. Chylack LT Jr, Wolfe JK, et al. The lens opacities classification system, version III (LOCS III). *Arch Ophthalmol.* 1993;111:831–836.
5. Wolf E, Gardiner JS. Studies on the scatter of light in the dioptric media of the eye as a basis of visual glare. *Arch Ophthalmol.* 1965;74:338–345.
6. Allen MJ, Vos JJ. Ocular scattered light and visual performance as a function of age. *Am J Ophthalmol.* 1967;44:717–727.
7. Sigelman J, Trokel SL, Spector A. Quantitative biomicroscopy of lens light backscatter. *Arch Ophthalmol.* 1974;92:437–442.
8. Brown NAP, Bron AJ, Ayliffe W, Sparrow J, Hill AR. The objective assessment of cataract. *Eye.* 1987;1:234–246.
9. Elliott DB, Hurst MA. Assessing the effect of cataract: a clinical evaluation of the Opacity Lensmeter 701. *Optom Vis Sci.* 1989;66:257–263.
10. Hockwin O, Sasaki K, Lerman S. Evaluating cataract development with the Scheimpflug camera. In: Masters BM, ed. *Noninvasive Diagnostic Techniques in Ophthalmology.* New York: Springer–Verlag; 1990:281–318.
11. Yager D, Liu C–L, Kapoor N, Yuan R. Relations between three measures of ocular forward light scatter and two measures of backward light scatter. In: *Technical Digest on Noninvasive Assessment of the Visual System* (O.S.A., Washington, DC) 1993;3:174–177.
12. Thurston GM, Hayden DL, Burrows P, et al. Quasielastic light scattering study of the living human lens as a function of age. *Curr Eye Res.* 1997;16:197–207.
13. Chylack LT Jr, Rosner B, Cheng H–M, McCarthy D, Pennett M. Sources of variance in the objective documentation of human cataractous change with Topcon SL-45 and Neitz-CTR retroillumination photography and computerized image analysis. *Curr Eye Res.* 1987;6:1381–1390.
14. van den Berg TJTP. Depth dependent forward light scattering by donor lenses. *Invest Ophthalmol Vis Sci.* 1996;37:1157–1166.
15. van den Berg TJTP. Light scattering by donor lenses as function of depth and wavelength. *Invest Ophthalmol Vis Sc.* 1997;38:1321–1332.
16. van den Berg TJTP, Spekreijse H. Light scattering model for donor lenses as function of depth. *Vision Res.* 1999;39:1437–1445.
17. van de Hulst HC. *Light Scattering by Small Particles*. New York: Dover Publications; 1981.
18. Willis CE, Bencomo JA. Logistic representation of the sensitometric response of screen-film systems: empirical validation. *Med Phys.* 1990;17:676–679.
19. van den Berg TJTP. Analysis of intraocular straylight, especially in relation to age. *Optom Vision Sci.* 1995;72:52–59.

Inhibition of Intraocular Tumor Growth by Topical Application of the Angiostatic Steroid Anecortave Acetate

Abbot F. Clark,[1] Jessamee Mellon,[2] Xiao-Yan Li,[2] Ding Ma,[2] Henry Leber,[2] Rajendra Apte,[2] Hassan Alizadeh,[2] Sushma Hegde,[2] Amanda McLenaghan,[2] Elizabeth Mayhew,[2] Thomas J. D'Orazio,[2] and Jerry Y. Niederkorn[2]

Purpose. This study examined the effect of an angiostatic agent on the growth of a highly vascularized intraocular tumor.

Methods. A murine uveal melanoma cell line (99E1) was transplanted intracamerally into athymic nude BALB/c mice. Mice were treated topically three times per day beginning on the day of tumor transplantation and continuing through day 28. Groups included (a) 1% anecortave acetate, (b) vehicle control, or (c) no treatment. Tumor growth was scored clinically according to the volume of anterior chamber occupied by tumor. Intraocular tumor weights were determined on days 10, 14, 21, and 28. The effect of the test agents on tumor cell proliferation was examined in vitro by [^{3}H]thymidine incorporation.

Results. Tumors grew progressively in untreated mice and mice treated with the vehicle; tumors filled the entire eye by day 20 and frequently perforated the globe by day 21. By contrast, tumors treated with anecortave acetate grew significantly slower ($P < 0.025$) and did not perforate the eye. On days 21 and 28 the net tumor weight of the AL-3789–treated animals was 40% to 30% of controls ($P < 0.05$). Tumor inhibition was presumably due to the angiostatic properties of anecortave acetate because the compound did not affect tumor cell proliferation in vitro.

Conclusions. The topical ocular administration of anecortave acetate restricted the growth of a highly vascularized angiogenic intraocular tumor. (*Invest Ophthalmol Vis Sci.* 1999;40:2158–2162)

Angiogenesis, the process in which new capillaries sprout from existing vessels, is crucial for embryonic development, growth, tissue repair, and certain disease processes.[1] The role of angiogenesis in the growth and metastasis of solid tumors is well recognized.[1] Recently, considerable effort has focused on the inhibition of angiogenesis as a strategy for controlling the growth and metastasis of various solid tumors.[1] A variety of agents have been proposed for inhibiting angiogenesis, including antagonists of vascular endothelial growth factor (VEGF) or VEGF receptors, fumagillin, α-interferon, and compounds that interfere with adhesion to cell matrices.[2]

The angiostatic steroids are an important class of angiostatic agents. These steroidal compounds were first described as being angiostatic in the chicken embryo chorioallantoic membrane (CAM) model of neovascularization, and angiostatic activity appeared to be independent of steroid hormone activity.[3] A new angiostatic steroid, anecortave acetate (AL-3789), recently has been demonstrated to have significant antiangiogenic activity in a wide variety of neovascular models, including the chick embryo CAM,[4] lipopolysaccharide-induced corneal neovascularization in the rabbit,[5] rat pup hypoxia-induced retinal neovascularization,[6] and retinopathy of prematurity in the kitten (Phelps DL, Collier RJ, and Clark AF, unpublished observation, November 1993).

The purpose of the present study was to determine whether topical ocular administration of anecortave acetate could inhibit the growth of an intraocular tumor. The tumor model was generated using the 99E1 transgenic tumor cell line that has been shown to be very rapidly growing and highly neovascular.[7,8]

Methods

Mice

Female athymic nude BALB/c (H-2^d) mice were purchased from The Jackson Laboratory (Bar Harbor, ME) and were incorporated into experiments when 8 to 10 weeks of age. The use of animals conformed to the ARVO Statement for the Use of Animals in Ophthalmic and Vision Research.

Tumor Cell Line

The 99E1 tumor cell line was derived from a choroidal/retinal pigmented epithelial ocular tumor that arose in a transgenic FVB/N mouse bearing the SV40 oncogene.[7] This tumor cell line expresses SV40 T antigen, as well as melanoma-associated antigens.[7,8] Tumor cells were cultured in Dulbecco's modified Eagle's medium (DMEM; GIBCO BRL, Grand Island, NY) containing 10% heat-inactivated fetal bovine serum (HyClone, Logan, UT), 1% L-glutamine (JRH Biosciences, Lenexa, KS), 1% sodium pyruvate, 1% vitamin solution, and 1% antibiotic-antimycotic solution (Biowittaker, Walkersville, MD). This tumor cell line was chosen for this study because of its similarity to human uveal melanoma and because it arose by in situ transformation within the uveal tract/retinal pigment epithelium of an FVB/n mouse.[7,8]

Intracameral Transplantation

A modified quantitative technique for the intracameral (IC) transplantation of precise numbers of tumor cells into the anterior segment of the mouse eye has been described previ-

From the [1]Alcon Laboratories, Inc., Fort Worth, Texas, and [2]Department of Ophthalmology, University of Texas Southwestern Medical Center, Dallas, Texas.

Submitted for publication July 9, 1998; revised February 11, 1999; accepted April 13, 1999.

Proprietary interest category: E, C_2.

Presented in abstract form at the annual meeting of the Association for Research in Vision and Ophthalmology, Fort Lauderdale, Florida, May, 1995.

Reprint requests: Abbot F. Clark, Alcon Laboratories, Inc., R2-41 6201 South Freeway, Fort Worth, TX 76134-2099.

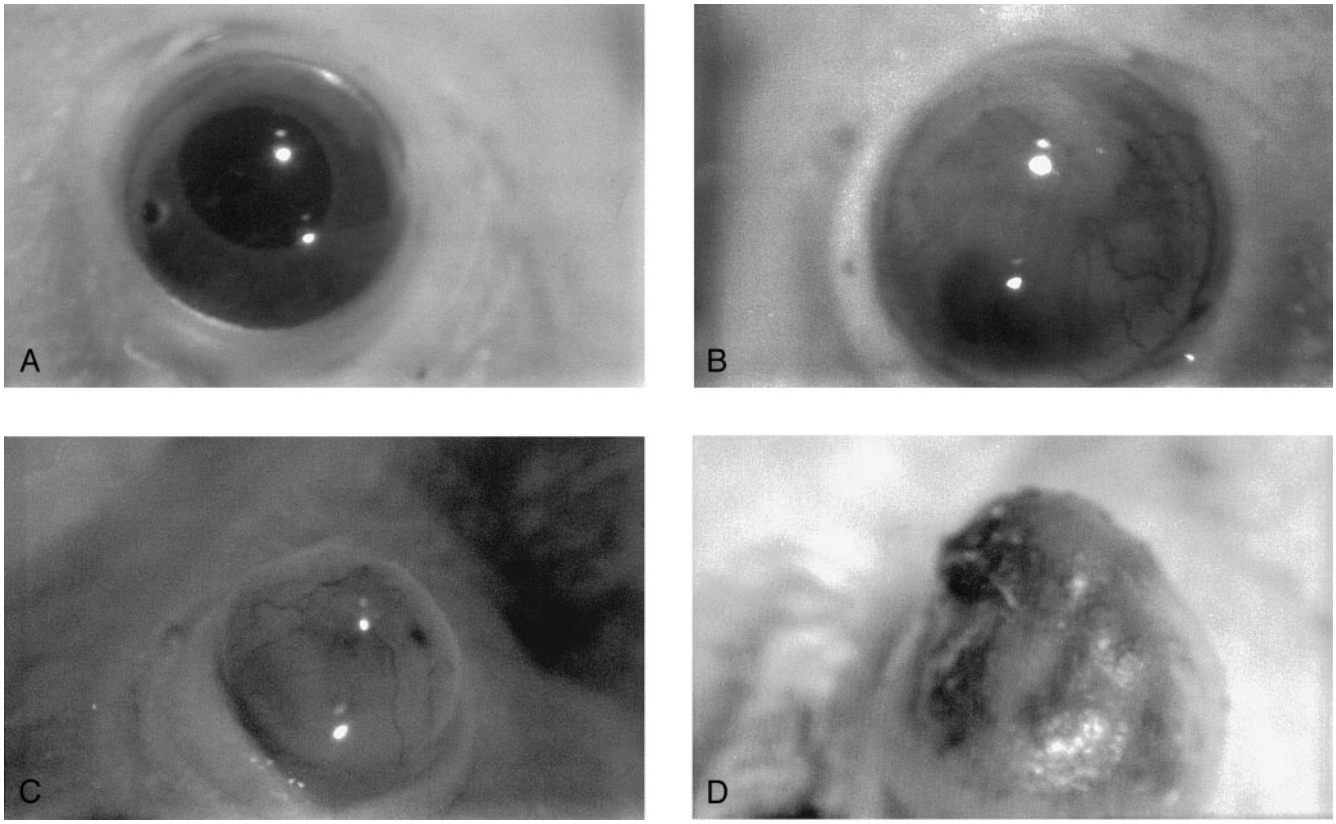

FIGURE 1. Clinical appearance of a typical intraocular 99E1 tumor treated topically with either anecortave acetate (**A**, **C**) or vehicle (**B**, **D**) on day 10 (**A**, **B**) or day 28 (**C**, **D**) after intracameral transplantation of 99E1 uveal melanoma cells.

ously.[8] Mice were deeply anesthetized with 0.66 mg ketamine hydrochloride (Vetalar; Parke, Davis, and Co., Detroit, MI) given intramuscularly. Tumor cells (10^5/5 μl) were inoculated into the anterior chamber, using a 1.0-ml Hamilton syringe fitted with a 35-gauge glass needle.

Preparation and Topical Administration of Anecortave Acetate

Anecortave acetate (AL-3789) [4,9(11)-pregnadien-11β,17α,21-triol-3,20-dione-21-acetate] was prepared as a proprietary 1% nonsettling suspension. Control animals received the same vehicle. Groups of animals (n = 5 to 10 mice/group) were treated three times a day with 4 μl of 1% anecortave acetate or with vehicle while a third group remained untreated.

Assessment of Tumor Mass

Eyes were examined two to three times per week using an operating microscope and the tumor growth scored based on the relative tumor mass that occupied the anterior chamber.[8] Tumor-containing eyes and the contralateral, normal eyes were enucleated at necropsy and weighed. The difference between the weight of the tumor-containing eye and the contralateral normal eye was considered to be an approximation of the tumor mass for each mouse.

Assay for In Vitro Tumor Cell deacetylated

The effect of anecortave acetate and its deacetylated metabolite on 99E1 tumor cell proliferation was assessed in vitro. 99E1 cells were suspended in complete DMEM (10^5 cells/ml), and 100 μl was added to each well in 96-well microtiter plates. One hundred microliters of DMEM containing anecortave acetate or its deacetylated metabolite (AL-4940) at 10^{-6} M or 10^{-7} M concentrations were added to each well. Cultures were incubated at 37°C for 24, 48, and 72 hours. During the final 18 hours of incubation, 1 μCi of [^{3}H]thymidine (Amersham Co., Arlington Heights, IL) was added to each well. Cells were harvested onto filter papers, using a MASH II cell harvester (MA Bioproducts, Walkersville, MD), and the incorporation of [^{3}H]thymidine was determined by liquid scintillation counting on a Beckman scintillation counter (Beckman Instruments, Inc., Irvine, CA).

Statistics

Longitudinal growth models were fit to the clinical score data plotted as the mean clinical score versus time. The slopes of the lines were compared by linear regression analysis. Statistical significance in tumor weights between experimental and control groups was determined by Student's *t*-test. Significance was assumed when $P < 0.05$.

RESULTS

As in previous studies,[8] 99E1 melanomas grew rapidly after IC transplantation. Intraocular tumors grew in all mice, although

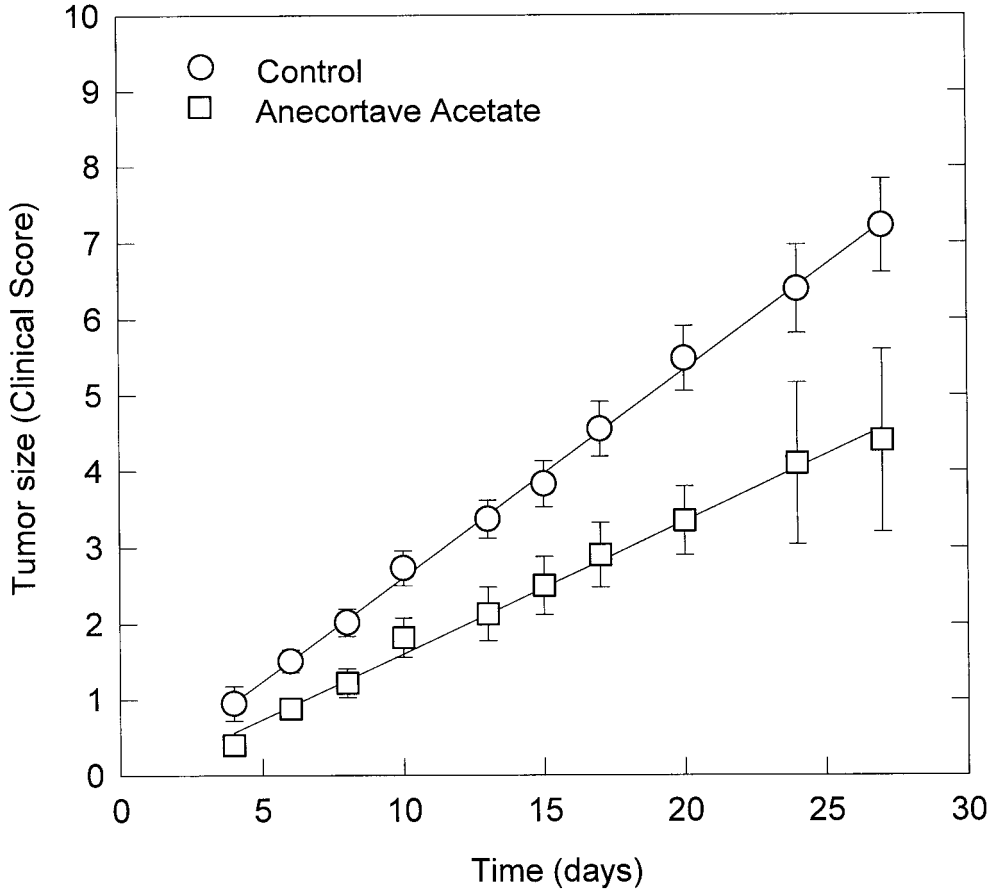

FIGURE 2. Clinical assessment (mean ± SEM) of the effect of topically applied anecortave acetate and vehicle on the intraocular growth of 99E1 tumors in BALB/c nude mice. Tumor growth rate in the anecortave acetate treated group was statistically slower than the growth rate in the control group ($P < 0.025$). $n = 9$ to 30 for the control group and $n = 5$ to 25 for the anecortave acetate treated group.

the extent of tumor growth varied between the treated and untreated groups. Tumor growth patterns in mice treated with the vehicle did not differ significantly from the untreated control group. Tumors perforated the globe of the eyes between days 21 to 28 in approximately one half (4/9) of the mice in the untreated and vehicle groups. However, topical application of anecortave acetate resulted in a marked inhibition of clinically assessed tumor growth (Figs. 1, 2). The growth rate of tumors in the control (vehicle and untreated) animals was significantly greater that the tumor growth rate in the anecortave acetate–treated group ($P < 0.025$). Tumors did not perforate the globe in any of the treated mice. These clinical observations were confirmed by weighing the tumor-containing eyes. Anecortave acetate treatment produced 44%, 40%, 61%, and 70% reductions in the tumor weights of the tumor-containing eyes on days 10, 14, 21, and 28 compared to their respective control groups ($P < 0.05$ for days 10, 21, and 28) (Fig. 3). Tumor weights (mean ± SEM in milligrams) for the control group were 6.26 ± 1.07 ($n = 10$) for day 10, 9.04 ± 2.55 ($n = 10$) for day 14, 43.03 ± 8.67 ($n = 11$) for day 21, and 110.7 ± 29.6 ($n = 9$) for day 21. Tumor weights in the anecortave acetate group were 3.49 ± 1.11 ($n = 10$) for day 10, 5.46 ± 3.20 ($n = 5$) for day 14, 16.72 ± 6.30 ($n = 5$) for day 21, and 32.62 ± 13.66 ($n = 5$) for day 28. The clinical scores appeared to underestimate the efficacy of anecortave acetate compared to the tumor weights most likely because the clinical scores were based on visual inspection of tumor size in the anterior segment and did not account for tumor growth in the posterior segment.

The inhibition of intraocular tumor growth was presumably due to the potent angiostatic properties of anecortave acetate although it was theoretically possible that this compound was either directly cytotoxic to tumor cells or inhibited tumor cell proliferation. However, the results from in vitro assays indicated that neither the active nor the deacetylated form of anecortave acetate affected the viability or the proliferation of 99E1 tumor cells over a 72-hour period (Fig. 4).

DISCUSSION

The growth of solid tumors is limited by the tumor's ability to obtain a nutritive source via stimulation of new blood vessel growth. Injection of 99E1 tumor cells into the anterior chamber of nude mice leads to a rapidly proliferating and highly neovascular tumor. Topical ocular administration of the angiostatic steroid anecortave acetate beginning at the time of injection of tumor cells led to a significant decrease (40%–70% inhibition) in tumor growth rate over the 4-week period of treatment. Neither anecortave acetate nor AL-4940 (the deacetylated metabolite) affected tumor cell proliferation in vitro, suggesting that this agent inhibited tumor growth by its angiostatic action.

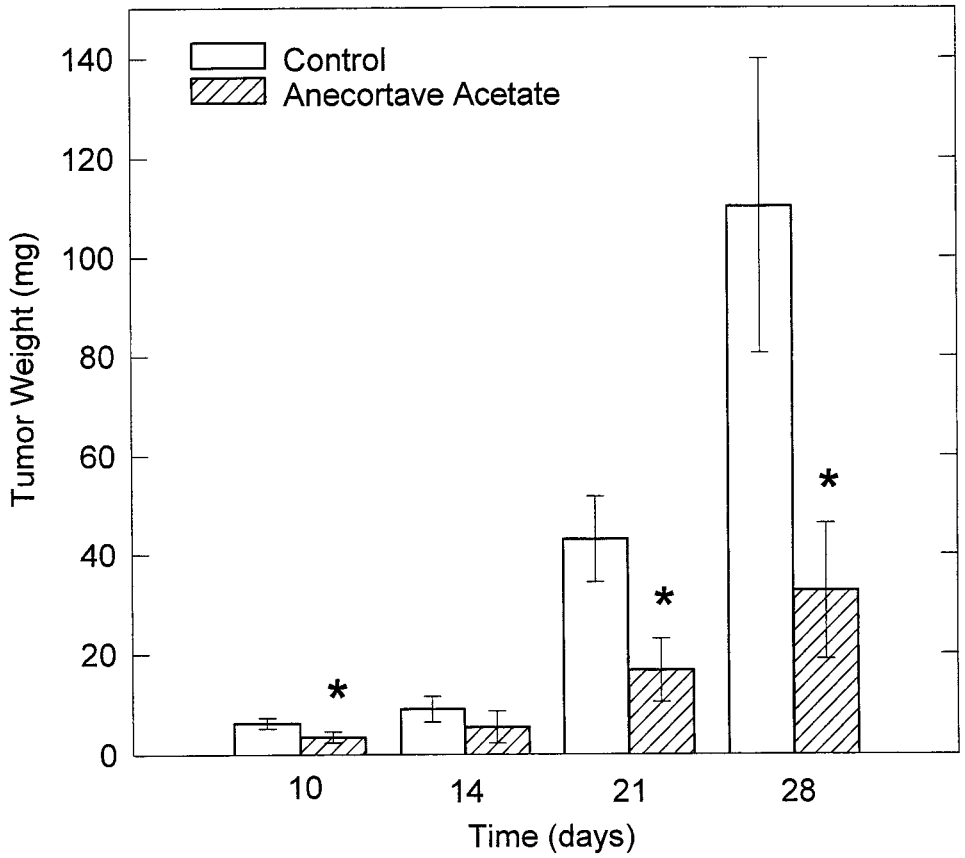

FIGURE 3. Effect of topically applied anecortave acetate on intraocular tumor mass (mean ± SEM). There were 5 to 11 mice per group. $^*P < 0.05$ for days 10, 21, and 28.

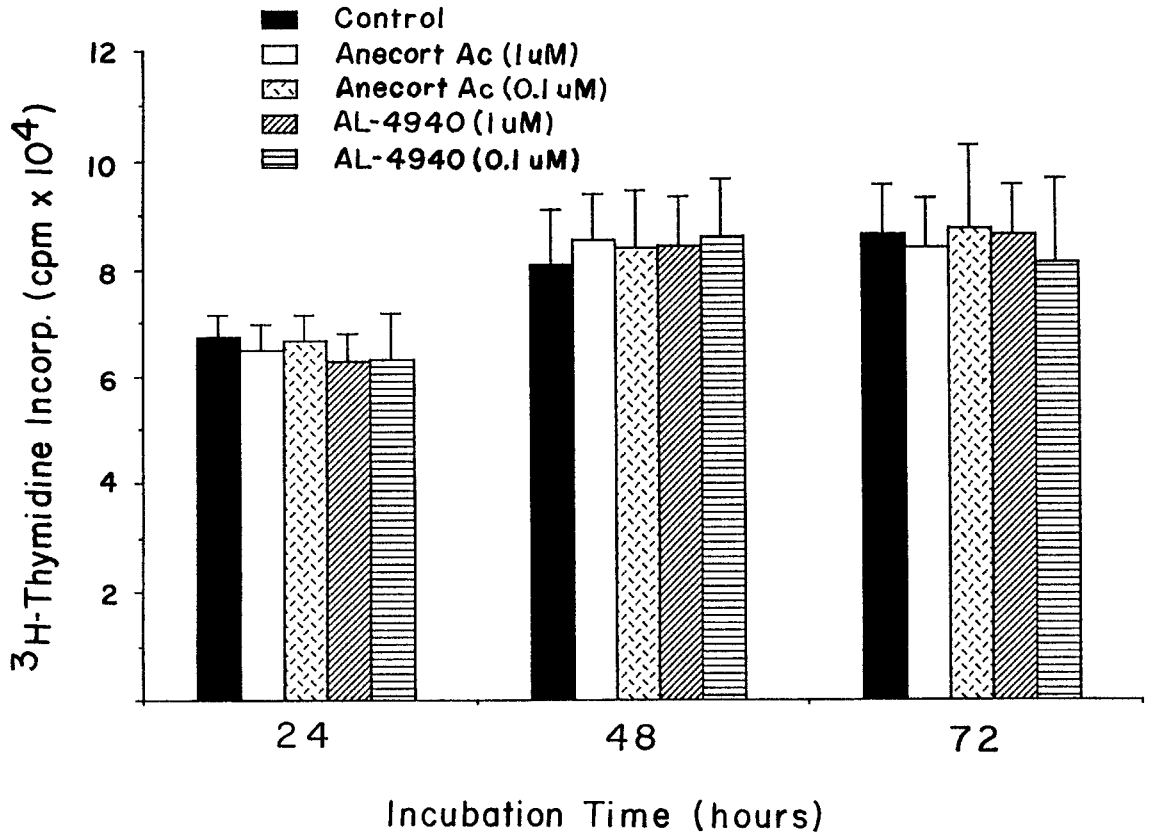

FIGURE 4. Effect of anecortave acetate (Anecort Ac) and its deacetylated metabolite AL-4940 on the proliferation of 99E1 tumor cells. Addition of either compound at 0.1 μm or 1 μm for 24 to 72 hours had no effect on tumor cell proliferation (mean ± SD, $n = 4$).

Anecortave acetate has been shown to have considerable angiostatic activity in several different neovascularization model systems. It is one of the more potent angiostatic steroids in the chicken embryo CAM model of neovascularization.[4] Topical ocular administration of anecortave acetate four times per day or two times per day almost totally inhibited LPS-induced corneal neovascularization in rabbits.[5] A single intravitreal injection of anecortave acetate into rat pups significantly inhibited hypoxia-induced retinopathy.[6] Likewise, a single intravitreal injection of AL-4940 into the eyes of kittens in a retinopathy of prematurity model caused a 50% reduction in retinal neovascularization compared to vehicle injected eyes (Phelps DL, Collier RJ, and Clark AF, unpublished observation November 1993).

Unlike many other angiostatic agents, it appears that anecortave acetate is angiostatic in a wide variety of neovascularization models, independent of the species, the tissue undergoing angiogenesis, and the initial angiogenic signal. Anecortave acetate is a 21-acetate ester that is deacetylated rapidly in the eye and blood. It displays effective ocular penetration when applied topically to the eye and therefore offers good bioavailability.[4] Other angiostatic steroids, such as medroxyprogesterone acetate, have been reported to inhibit urokinase plasminogen activator (uPA) activity[9,10] and upregulate plasminogen activator inhibitor (PAI) expression.[10] One of the rate-limiting steps in angiogenesis consists of an angiogenic signal-mediated stimulation of vascular endothelial cell (VEC) uPA activity to enable the VECs to break through the vessel basement membrane and migrate through interstitial tissue toward the angiogenic signal (i.e., the tumor). At least a portion of anecortave acetate's angiostatic activity appears to be due to the inhibition of vascular endothelial cell uPA and stromelysin expression (DeFaller JM, McNatt LG, and Clark AF, unpublished observation), as well as the upregulation of PAI expression in the retinas of rats in a model of retinopathy of prematurity.[11]

There are a number of ocular diseases in which neovascularization plays a major role in the loss of vision. It is our hope that new angiostatic agents will be discovered that significantly interfere with ocular neovascularization and thereby preserve vision. Although anecortave acetate is active in a variety of neovascular animal models, including the inhibition of intraocular tumor growth shown in the present study, further evaluation is required to determine whether it will be useful for preserving vision in humans.

Acknowledgment

The authors thank Mark Von Tress for his biostatistical analysis of our data.

References

1. Folkman J. Angiogenesis in cancer, vascular rheumatoid and other disease. *Nat Med.* 1995;1:27–30.
2. Moses MA, Langer R. Inhibitors of angiogenesis. *Bio/Technology.* 1991;9:630–634.
3. Crum R, Szabo S, Folkman J. A new class of steroids inhibits angiogenesis in the presence of heparin or a heparin fragment. *Science.* 1985;230:1375–1378.
4. Clark AF. AL-3789: a novel ophthalmic angiostatic steroid. *Exp Opin Invest Drugs.* 1997;6:1867–1877.
5. BenEzra D, Griffin BW, Maftzir G, Sharif NA, Clark AF. Topical formulations of novel angiostatic steroids inhibit corneal neovascularization. *Invest Ophthalmol Vis Sci.* 1997;38:1954–1962.
6. Tolman BL, Collier RJ, Clark AF, Penn JS. Effects of an angiostatic steroid on neovascularization in the rat model of ROP [ARVO Abstract]. *Invest Ophthalmol Vis Sci.* 1995;36(4):**S**93. Abstract nr 454.
7. Anand R, Ma D, Alizadeh H, et al. Characterization of intraocular tumors arising in transgenic mice. *Invest Ophthalmol Vis Sci.* 1994;35:3533–3539.
8. Ma D, Comerford S, Bellingham D, et al. Capacity of simian virus 40 T antigen to induce self tolerance but not immunological privilege in the anterior chamber of the eye. *Transplantation.* 1994;57:718–725.
9. Ashino–Fuse H, Takano Y, Oikawa T, Shimamura M, Iwaguchi T. Medroxyprogesterone acetate, an anti-cancer and anti-angiogenic steroid inhibits the plasminogen activator in bovine endothelial cells. *Int Cancer J.* 1989;44:859–864.
10. Blei F, Wilson EY, Mignatti P, Rifkin DB. Mechanism of action of angiostatic steroids: suppression of plasminogen activator activity via stimulation of plasminogen activator inhibitor synthesis. *J Cell Physiol.* 1993;155:568–578.
11. Bullard LE, Rajaratnam VA, Collier RJ, Clark AF, Penn JS. AL-3789 inhibits retinal neovascularization in an animal model of ROP by inducing retinal PAI-1 [ARVO Abstract]. *Invest Ophthalmol Vis Sc*i. 1999;40(4):S619. Abstract nr 3255.